Czech University of Life Sciences

Faculty of Agrobiology, Food and Natural resources

Department of Veterinary Sciences

Development and optimization of the properties of binding proteins recognizing specific cytokines and their receptors

Diploma thesis

Autor of thesis: Bc. Johana Roubalíková Erbsová

Study programme: Conservation and Use of Natural Resources

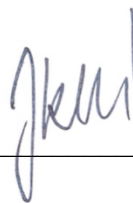**Thesis supervisor: RNDr. Pavla Postlerová, Ph.D.**

Thesis consultant: prof. Ing. Bohdan Schneider, CSc., DSc.

Čestné prohlášení

Prohlašuji, že svou diplomovou práci "Vývoj a optimalizace vlastností vazebných proteinů rozpoznávajících specifické cytokiny nebo jejich receptory" jsem vypracovala samostatně pod vedením vedoucího diplomové práce a s použitím odborné literatury a dalších informačních zdrojů, které jsou citovány v práci a uvedeny v seznamu literatury na konci práce. Jako autorka uvedené diplomové práce dále prohlašuji, že jsem v souvislosti s jejím vytvořením neporušila autorská práva třetích osob.

V Praze dne 14. 4. 2023   _____

Poděkování

Ráda bych na tomto místě poděkovala panu prof. Ing. Bohdanovi Schneiderovi, CSc., DSc., za jeho velkou podporu a pomoc během zpracovávání této práce, za možnost jejího vzniku a za cenné odborné připomínky a rady. Dále bych chtěla poděkovat své paní vedoucí, RNDr. Pavle Postlerové, Ph.D. za její neutuchající trpělivost, vlídný přístup během sepisování práce a za přínosné odborné připomínky a také RNDr. Marošovi Huličiakovi Ph.D. za vedení experimentální části této práce, možnost získání cenných a zajímavých zkušeností ze světa proteinového inženýrství a za hodnotné rady v procesu zpracovávání této práce. V neposlední řadě bych ráda poděkovala celému kolektivu Laboratoře biomolekulárního rozpoznávání za přátelské pracovní prostředí a samozřejmě také svojí rodině a přátelům.

Vývoj a optimalizace vlastností vazebných proteinů rozpoznávajících specifické cytokiny nebo jejich receptory

Souhrn

Cytokiny jsou signální proteiny, které hrají důležitou roli v imunitním systému. Cytokiny modulují signální dráhy nebo genovou expresi cílových buněk tím, že se vážou na specifické receptory. Schopnost detekce jejich množství v organismu může přispět k odhalení progrese některých civilizačních onemocnění, jako je například ateroskleróza, rakovina, revmatoidní artritida, astma a další.

Za účelem léčby a diagnostiky zmíněných onemocnění jsou často využívány tradiční protilátky, které ale vykazují řadu problematických vlastností. Tyto důvody vedly k vývoji proteinových "scaffoldů" (z anglického výrazu scaffold), které mohou částečně nahradit tradiční protilátky díky svému lepšímu chování. Proteinové "scaffoldy" jsou malé, zpravidla monomerní proteiny, které vykazují stabilní strukturu, lepší schopnost penetrovat buněčné membrány, a navíc díky možnosti jejich produkce v *Escherichia coli* jsou cenově dostupnější alternativou tradičních protilátek. Proteinové "scaffoldy" je možné trénovat k vazbě cílových, typicky proteinových molekul, a to systematickými mutacemi aminokyselin pomocí různých metod řízené evoluce, mezi které patří fágový, ribozomální nebo kvasinkový displej, error-prone PCR nebo *in silico* design.

Tato práce se zabývá vývojem druhé generace proteinových "scaffoldů" cílících na klinicky důležitý Interleukin-10 (IL-10) metodami řízené evoluce a popisem vazebných charakteristik. Pro účely stanovení vazebné afinity byl vypěstován IL-10 prostřednictvím buněčné linie Schneider 2 cells.

Druhá generace proteinových "scaffoldů" byla odvozena z parentálních klonů F5_WT a G3_WT, které byly vyvinuty v Laboratoři biomolekulárního rozpoznávání Biotechnologického ústavu Akademie Věd České republiky. Vazebná afinita výsledného proteinového scaffoldu F5_A2 druhé generace k IL-10 byla stanovena pomocí termoforézy v mikroskopickém měřítku (MST).

Klíčová slova: Error-prone PCR, proteinový scaffold, ELISA, IL-10, řízená evoluce

Development and optimization of the properties of binding proteins recognizing specific cytokines and their receptors

Summary

Cytokines are signaling protein molecules playing an important role in the immune system. Cytokines modulate signaling pathways or gene expression in target cell by binding to specific cellular receptors. Ability to determine amount of cytokines can contribute to detection of progression of some civilizational diseases such as atherosclerosis, cancer, rheumatoid arthritis, asthma, and others.

Antibodies used traditionally for treatment and diagnosis of the mentioned diseases provide several problematic properties. This led to development of protein scaffolds, which can partially replace traditional antibodies because of their improved behavior. Protein scaffolds are small, usually monomeric proteins that show stable structure, better cell membrane penetration ability and better affordability because of *Escherichia coli* production possibility. The scaffold molecules can be trained to bind to new target molecules, typically other proteins by systematic mutations of amino acid residues by various methods of directed evolution such as phage, ribosome, yeast display, by error-prone PCR, or by *in silico* design.

In this thesis, the second generation of protein scaffold derived binders targeting the clinically important Interleukin-10 (IL-10) was developed using directed evolution methods. For determination of binding affinity of modified scaffolds, IL-10 was produced via Schneider 2 cells insect cell line.

The second generation of protein scaffolds was derived from parental variants of F5_WT and G3_WT, which were developed in Biomolecular Recognition Laboratory of the Institute of Biotechnology of the Academy of Sciences of the Czech Republic. Binding affinity of the resulting second-generation protein scaffold F5_A2 to IL-10 was determined by microscale thermophoresis (MST).

Keywords: Error-prone PCR, protein scaffold, ELISA, IL-10, directed evolution

Table of contents

1 Introduction

Cytokines are proteins, glycoproteins or peptides influencing cell growth, proliferation, moving, behavior, and survival of the cells. Via cytokines, also called signaling molecules, cooperation and communication between immunity system cells is realized (Striz & Holan 2015). This phenomenon leads to fact that cytokines can influence the immunity system balance which is crucial for averting the development of pathological conditions that can result in several diseases (Ramani *et al*. 2015). Accurate quantification of cytokines is essential for understanding the immune health, moreover it allows physicians to initiate or adjust treatment for many diseases in a timely manner, such as cardiovascular disease (responsible for 17.9 million deaths annually), cancer (causing 10 million deaths annually) (www.who.com, 2022, online) and also depression, rheumatoid arthritis, AIDS, sepsis, and other chronic diseases (Liu *et al*. 2021).

Despite the extensive use of antibodies in therapeutic applications and cytokine detection in the treatment or prevention of the mentioned diseases, there are still a number of disadvantages associated with them (Liu *et al*. 2021; Lai & Dong 2016). These disadvantages, including, for example, their large size, limited tissue penetration capacities and high production costs, have prompted researchers to explore antibody alternatives called protein scaffolds (Luo *et al*. 2022).

Protein scaffolds are small and usually monomeric proteins, offering great stability, affinity, and better affordability because of production via *Escherichia coli* possibility. The production of protein scaffolds is, among other things, more environmentally friendly than the production of traditional antibodies, which are produced by bleeding animals (Nossal 1967). By utilizing methods of protein engineering, protein scaffold can be trained for desired properties optimization (Gebauer & Skerra 2020).

In this diploma thesis, second generation of protein scaffolds targeting clinically important interleukin 10, was made via directed evolution methods. Second generation protein scaffold library was derived from parental protein scaffold 57aBi clones F5 and G3, developed in Laboratory of Biomolecular recognition in Institute of Biotechnology, Czech Academy of Sciences in Vestec (Pham *et al*. 2021).

2 Objectives of the thesis

- Production of interleukin 10 via Schneider 2 insect cell line
- Create diversified DNA library derived from the 57aBi protein scaffold derived F5_WT and G3_WT variants by error-prone PCR method
- From these second-generation variants, select variants derived from F5 and G3 variants that bind interleukin 10 through ribosome display technique
- Screen the selected variants by ELISA binding assay
- Determine the binding affinity of the best second-generation F5 and G3 variants to interleukin 10 by using microscale thermophoresis measurement

3 Literature part

3.1 Mammalian cytokines and their receptors

One of the oldest mentions about cytokines comes from 1965 (Kasakura and Lowenstein 1965). Cytokines can be defined as cell-signaling proteins, glycoproteins or peptides which influence cell growth, differentiation, motion, behavior, or survival. Cytokines bind to their specific receptor and induce cell-signaling pathway and gene expression changes (Striz and Holan 2015). They are referred to as the most important signal and effector molecules in immune system (Ouyang & O'Garra 2019). Cytokines are divided into several groups including interferons, chemokines, interleukins, and tumor necrosis factor (Ferreira *et al.* 2019).

Interferons (IFNs) are cytokines with antiviral and immunomodulation effects. Based on chromosomal localization and structure, IFNs can be divided into three classes: I-IFN, II-IFN and III-IFN (Striz & Holan 2015). Antitumor effects of IFNs have been also provided in some recent studies (Lee *et al.* 2021; Jiang *et al.* 2020).

Chemokines are low molecular weight cytokines which can easily enter parenchyma and bind to various receptors expressed in several cell populations. Because of their chemokinetic activity, chemokines regulate supplement of inflammatory cells via concentration gradient during immune response or tissue damage, so they can mediate migration of cells in physiological conditions (Striz & Holan, 2015; Lacy 2015). Based on cysteine N-terminal localization, chemokines can be divided into four families: CXC, CC, CX3X, and XC (Fernandez & Lolis 2002). Chemokines were successfully used for immunotherapy anticancer treatment and for therapy of solid tumors (Propper & Balkwill 2022).

Tumor necrosis factor (TNF) is superfamily of approximately 50 membrane or soluble proteins. The most described member of TNF superfamily is a trimeric TNFα operating in pleiotropy and pro-inflammatory pathways and can also dispose of wide range of effects. TNFα has important role in immunopathology reactions or defensive mechanisms of the cells too (Striz & Holan 2015).

Interleukins is group of glycoproteins with various functions and structures with anti-inflammatory and pro-inflammatory behavior. First interleukin known as IL-1β was discovered by Igal Gery in 1972 (Gery & Waksman 1972). Because of initial consideration that interleukins (ILs) are produced by leukocytes, this large section of cytokines got its name as interleukins. Later it was proved that interleukins are produced by many other cells of mammalian organism, such as macrophages, endothelial or epithelial cells, dendritic cells, and muscle cells. Main functions of ILs' include growth modulation, differentiation, or initiation in processes of immune reaction or inflammation (Justiz & Qurie 2022). Thanks to high affinity of ILs' to their

receptors, they can affect many tissue reactions in cells (Ferreira *et al.* 2019; Striz & Holan 2015). Nowadays, 40 types of ILs' have been described (Ferreira *et al.* 2019) and divided into several ILs' families: IL-1 family, IL-2 family, IL-6 family, IL-10 family, IL-12 and IL-17 family (Gajdacs *et al*. 2021). Studies of interleukins are used for investigation of reaction processes linked to clinical medicine and insight of interleukins effects mechanisms can improve efficiency of targeting therapeutic treatment of significance diseases of civilization such as cancer, cardiovascular diseases, diabetes, asthma, or rheumatoid arthritis (Liu *et al*. 2021).

3.2 Interleukin 10 family

Apart from the most studied immunosuppressive cytokine IL-10, this family includes IL-9, IL-20, IL-22, IL-24, IL-26, IL-28, and IL-29 (Striz & Holan 2015).

3.2.1 Interleukin 10 and its clinical significance

The major member of IL-10 family and major immunosuppressive cytokine, IL-10, was identified in 1989 by T. R. Mosmann and his colleagues (Fiorentino *et al.* 1989). Initially IL-10 was described as factor produced by Th2 cells inhibiting Th1 cells cytokines. Due to this fact, IL-10 was originally named as cytokine synthesis inhibiting factor. Except for ability of Th2 cells cytokines inhibition, IL-10 proves suppression of inflammation reaction and can regulate differentiation and proliferation of T and B lymphocytes, granulocytes, or NK cells (natural killer cells). IL-10 also reduces MHC II (major histocompatibility complex class II) molecules expression, involving the recognition of foreign structures (Striz & Holan 2015; Ouyang *et al.* 2011). IL-10 consists of two chains of 160 amino acids formed into non-covalent linked helix homodimer which recognizes IL-10 membrane receptor (IL-10R) composed of two α and β chain subunits. IL-10 first binds specifically to the alpha subunit, which leads to conformation change and binding to the beta subunit. Receptor then transmits the signal into the cell via activation of JAK1/STAT3 (Janus kinases 1/ signal transducer and activator of transcription 3) signaling pathway, when STAT3 homodimers are phosphorylated and subsequently translocated right to the nucleus for stimulating target genes expression. (Hutchings *et al.* 2013; Verma *et al.* 2016). Production of IL-10 is ensured by monocytes, macrophages and T leukocytes, B leukocytes, neutrophils, mast cells, dendritic cells, or NK cells (Hutchings *et al.* 2013).

IL-10 is associated with development and progression of many types of civilization diseases such as cardiovascular disease (CVD) or cancer which causes over a 27.9 million deaths a year (www.who.com, 2022, online).

IL-10 provides strong anti-inflammatory effects and can inhibit some pro-inflammatory cytokines (IL-6, IL-8, TNF, activated macrophages etc.). During development of one of the most common types of CVD - atherosclerosis, inflammation plays a crucial role. IL-10 may prevent the expression of key pro-inflammatory molecules - for example oxidated phospholipids or activated macrophages, which can increase oxidative stress even more and promote cell death that develop the atherosclerotic plaque and other pro-atherosclerotic inflammatory processes (Bagchi *et al.* 2020). It has been proved, that low level of IL-10 in blood plasma leads to progression of unstable atherosclerotic plaques, which can cause an acute thrombosis (Fernandez & Kaski 2002). On the other hand, elevated blood plasma level of IL-10 is associated with many types of tumor development. IL-10 may be considered as important cancer development factor. IL-10 can be also produced by cancer cells themselves (Mirlekar 2022; Labani-Motlagh *et al.* 2020). This phenomenon leads to unbalance between pro-inflammatory and anti-inflammatory molecules and homeostasis disruption (Gonzalez-Garta *et al.* 2021). Several studies have pointed out that IL-10 increases proliferation and survival of tumor cells. Blocking of IL-10 may increase effects of NK cells which are important for tumor immune response (Mirlekar 2022). Recently, some studies are focusing on increasing level of IL-10 in specific localization of tumor microenvironment, because of tumor specific immunity activation, which is mediated by IL-10 dependent cytotoxic T lymphocytes (Rallis *et al*. 2021).

3.2.1.1 Other members of IL-10 family and its clinical significance

IL-19 with molecular weight 21 kDa is an anti-inflammatory cytokine produced mainly by monocytes (Vaillant & Qurie 2021). IL-19 is bound by heterodimer receptor consisting of IL-20α and IL-20β subunits and by this signaling pathway including STAT3 is activated. Apart from immune cells, IL-19 occures in epithelial cells, vascular smooth muscle cells or in endothelial cells (Striz & Holan 2015). Because artery endothelial disruption of functionality is one of initial mechanisms triggering oxidative stress leading to atherosclerosis rise and development, IL-19 may present a promising atherosclerosis biomarker and potential therapeutic atherosclerosis target (Chen *et al.* 2021).

IL-20 is proinflammatory cytokine with molecular weight 21 kDa, it is produced mainly by monocytes and keratinocytes. IL-20 is bounded by heterodimer receptor composed of IL-20R1 and IL-20R1 subunits. Signaling effects of IL-20 is leading through STAT3 activation to expression of many proinflammatory genes - for example TNFα. High levels of IL-20 are associated to skin inflammation or psoriasis. Recent study of local inflammatory effects in arthritic disease of IL-20 have been provided. IL-20 is important cytokine that may stabilize the

imbalance between pro and anti-inflammatory molecules for homeostasis establishment (Kragstrup *et al.* 2018; Striz & Holan 2015).

IL-22 is produced mainly by T lymphocytes Th17 and Th22, also by innate lymphomas cells and it´s molecular weight is about 19-22 kDa. IL-22 plays a defensive role during bacterial infection of lung epithelial cells and digestive tract, also coordinates adaptive and humoral immune reaction (Dudakov *et al.* 2015). IL-22 is bound by heterodimer receptor complex composed of two IL-22R and IL-10R2 subunits. When IL-22 is specifically bound to its receptor, signaling pathway including JAK1, tyrosine kinase 2 and STAT3 is activated. By IL-22 signalization stimulation of proinflammatory cytokines and growth of hepatocytes and epithelial cells are activated (Striz & Holan 2015). It was provided, IL-22 production is stimulated by tumor cells, which may indicate IL-22 as therapeutic target (Markota *et al*. 2018).

IL-24 was initially described as melanoma differentiation-associated protein with tumor suppression effects and its molecular weight is 19 kDa. Production of IL-24, stimulated by other proinflammatory cytokines, comes mainly from monocytes, macrophages and Th2 lymphocytes. IL-24 occurring via JAK/STAT signal transduction pathway, signals through heterodimer receptors IL-20R/IL-20R2 and IL-22R1/IL-20R. In higher concentrations, IL-24 can cause malignant cells apoptosis (Persaud *et al.* 2016; Striz & Holan 2015) which can be crucial for finding anticancer treatment strategies (Menezes *et al.* 2014; Menezes *et al.* 2018). Recent study provided increased urine and blood level of IL-24 after acute kidney injury (AKI), which may suggest IL-24 as a promising biomarker of AKI (Tabata *et al.* 2020).

IL-26 is an inflammatory cytokine produced by T-lymphocytes Th17 and through signaling via STAT1 (signal transducer and activator of transcription 1) and STAT3 stimulates IL-10 and IL-8 production. IL-26 is bound through heterodimer receptors IL-20R/IL-20R2 and IL-22R1/IL-20R. Currently IL-26 is considered as a novel biomarker for disease activity assessment in systemic lupus erythematosus (Brilland *et al.* 2021; Vaillant & Qurie, 2021).

IL-28 is antiviral defensive cytokine which occurs in two forms - IL-28A and IL-28B. IL-28 is produced by T lymphocytes and viral-infected dendritic cells, and it is bound by IL-28 receptor composed of IL28αR and IL-10βR subunits. Because IFNγ promotion effects, plays IL-28 an important role in adaptive immunity (Vaillant & Qurie 2021; Striz & Holan 2015). Recent study suggest that IL-28 may be a promising biomarker for mortality prediction in traumatic patients with sepsis (Yang *et al.* 2022).

IL-29 is also classified as interferon because it has antiviral efficiency and its molecular weight is about 19-24 kDa. IL-29 is produced by cells infected by virus, T lymphocytes and dendritic cells (Vaillant & Qurie 2021; Striz & Holan 2015). Apart from therapeutic use in patients with chronic hepatitis C because of IL-29 high expression in liver cells of infected

patients (Striz & Holan 2015), IL-29 can be also used as diagnostic factor of rheumatoid arthritis (Rocha-Junior *et al.* 2020).

3.3 Protein scaffolds derived from small protein domains

Although engineered protein antibodies are considered crucial entity for usage in huge field of therapy, diagnosis and research, protein binding entities called protein scaffolds present promising competitive alternative (Ahmadi *et al.* 2021). Some of developed protein scaffolds have already passed preclinical or clinical studies, for example Affibody molecules, such as (111)I-ABY-025 reengineered for breast cancer metastases imaging via HER2 (human epidermal growth factor receptor 2 targeting) (Sörensen *et al.* 2014), or (188)Re-ABY-251 for ensuring therapy of oncology metastatic patients (Liu *et al.* 2022).

The main reasons leading to protein scaffold development are high production cost, large size and narrow tissue penetration ability of engineered antibodies. The primary benefits of small-domain derived scaffolds include their small size and no posttranslational modification necessity, which leads to prokaryotic production possibility and better financial availability (Ahmadi *et al.* 2021; Luo *et al.* 2022). Overview of already constructed protein scaffolds is listed in Table 1.

Protein scaffold is defined as „organizing platform that links together at least two protein partners" (Lemmens *et al.* 2020), it could be also described as „small protein with stable tertiary structure and mutable residues" (Luo *et al.* 2022).

Protein scaffold mostly contains two fragments, which are corresponding to antibodies (Luo *et al.* 2022). The first fragment, termed as the constant one, consists of alpha helixes or beta sheets and supports the conformational stability. The second fragment is termed as the variable one, it consists of uncovered loops or some secondary structure residues and supplies the specific binding capacity through receptor-ligand binding or chemical forces. Also, 20-10 amino acids residues of the variable fragment can be randomized for the new affinity binder acquired (Hosse *et al.* 2006; Luo *et al.* 2022).

3.3.1 Role of protein scaffolds in protein therapy and diagnostics

Protein scaffolds present an alternative possibility for therapeutics and diagnostics. The benefits of small-domain derived scaffolds include, as mentioned above, their small size and better financial affordability because of the possibility of production in prokaryotic cells (*E. coli*). Among other benefits, possibility of *E. coli* production of 57aBi (Pham *et al.* 2021) that provides posttranslational glycosylation of the protein is decreased, also decreases the resulting protein scaffold variability (Wang *et al.* 2013). Moreover, they can be used for cancer diagnostic visualizing, intracellular transport, signaling pathway block or elimination of

microbes (Luo *et al*. 2022). It is excepted that protein scaffolds could provide relatively cheap, safe, and accessible drugs with therapeutic effectiveness. (Gebauer & Skerra 2020; Vazquez-Lombardi *et al*. 2015; Luo *et al*. 2022).

3.3.2 Development of 57aBI scaffold

In Laboratory of Biomolecular recognition, Institute of Biotechnology in Vestec, robust antibody protein called 57aBi was engineered (Pham *et al*. 2021). From the Protein Data Bank, 12 potentional IL-10 binder candidates were chosen. These IL-10 binder candidates were supposed to fulfil the criteria including small size, possibility of its soluble form in *E. coli* and sufficiently high-resolution monomeric X-ray structure. After this initial search, the best candidates were subdued to another selection for protein scaffold. Obtained protein candidates were supposed to provide non-toxicity, non-immunogenicity, thermostability, tolerance to mutations and high specificity. The final protein candidate contained 10 easily mutable surface patches, elements for ribosome display selection, Strep-tag at the N-terminus for affinition chromatography and the C-terminus c-myc detection tag.

Molecular weight of 57aBbi is 15 kDa, which is about ten times smaller than the average size of a classical antibody. This fact leads to better penetration of 57aBi through the tissuesand better modulation of cell signaling pathways that can modulate development of many diseases by using them as inhibitors of specific cytokines. From the obtained 57aBi wild type two clones called F5_WT and G3_WT were selected via 5 rounds of ribosome display and ELISA screening, which furnish the best affinity to IL-10 reaching up to 6 nM value of dissociation constant (Pham *et al*. 2021).

Table 1: Overview of small protein scaffolds, their targeting and derived structures (Luo et al. 2022; Miles et al. 2021; Gebauer and Skerra 2020; Simeon and Chen, 2018; Skrlec et al. 2015).

Name of a scaffold	Molecular weight (kDa)	Target	Derived structure (PDB ID)	Molecular weight of derived structure (kDa)	Literature
Affibody	6.5	HER 2	2M5A	13.04	Lindborg *et al.* 2013
			3MZW	76.38	Eigenbrot *et al.* 2010
			5EFW	30.80	Wang *et al.* 2016
			2OTK	19.97	Hoyer *et al.* 2008
			1Q2N	6.65	Zheng *et al.* 2004
			1LP1	13.50	Högbom *et al.* 2003
Affimer	11	IL-6	1NB5	147.14	Jenko *et al.* 2003
			5AOO	90.23	Sabin and Plevka, 2016
ANTICALIN®	18-20	VEGF	4GH7	105.92	Gebauer *et al.* 2013
			5N47	157.69	Schiefner *et al.* 2018
			4MVI	25.87	Rauth *et al.* 2016
			5NKN	20.34	Barkovskiy *et al.* 2019
Adnectin/ monobody	10	VEGFR-2	1TTG	9.95	Main *et al.* 1992
			3QWQ	87.64	Ramamurthy *et al.* 2012
			5N7E	35.02	Reckel *et al.* 2017
			3QWR	66.66	Ramamurthy *et al.* 2012
			2OCF	47.2	Koide *et al.* 2002
			3RZW	43.32	Koide *et al.* 2012
			3UYO	23.87	Koide *et al.* 2012
Knottin	<4	Calcium channels	2IT7	2.91	Heitz *et al.* 2008
Kunitz	7	Human neutronphil elastase	1KTH	6.83	Arnoux *et al.* 2002
Avimer	4	HER4	1AJJ	4.21	Fass *et al.* 1997
Centyrins	10	EGFR	5L2H	46.07	Goldberg *et al.* 2016
			3TES	43.00	Jacobs *et al.* 2012
Affilin	20	HER 2	1UBI	8.58	Ramage *et al.* 1994
	10	EGFR	2JDG	21.82	Ebersbach *et al.* 2007
DARPins	14-21	VEGF, HGF, VEGF- A	5KNH	30.61	Teplyakov *et al.* 2017
			4YDY	66.26	Oblomova *et al.* 2015
			4HRL	40.77	Jost *et al.* 2013
			4LNU	157.23	Cao *et al.* 2013
			1MJ0	18.05	Kohl *et al.* 2002
			4JB8	50.38	Seeger *et al.* 2013

HER2: human epidermal growth factor receptor 2; VEGF: Vascular endothelial growth factor; VEGFR-2: vascular endothelial growth factor receptor 2; HER4: human epidermal growth factor receptor 4; EGFR: Epidermal growth factor receptor; HGF: Human growth factor; VEGF-A: Vascular endothelial growth factor A.

3.4 Directed evolution of proteins

Directed evolution is defined as "Synthetic process that harnesses the power of selection to evolve molecules, typically proteins or nucleic acids, from large, stochastically permuted pools or combinatorial libraries, to have desired properties" (Gold *et al*. 2013). Directed molecular evolution of proteins consists of two primary steps: diversification and selection. Initially, a vast and varied DNA library is created from the original (wild type) gene encoding the protein of interest to diversify it. Following this, proteins with desired characteristics are selected from this novel protein library which has been encoded by the generated diverse DNA library (Ren *et al*. 2019; Matsuura *et al*. 2006). Diagram of directed evolution process is depicted in Figure 1.
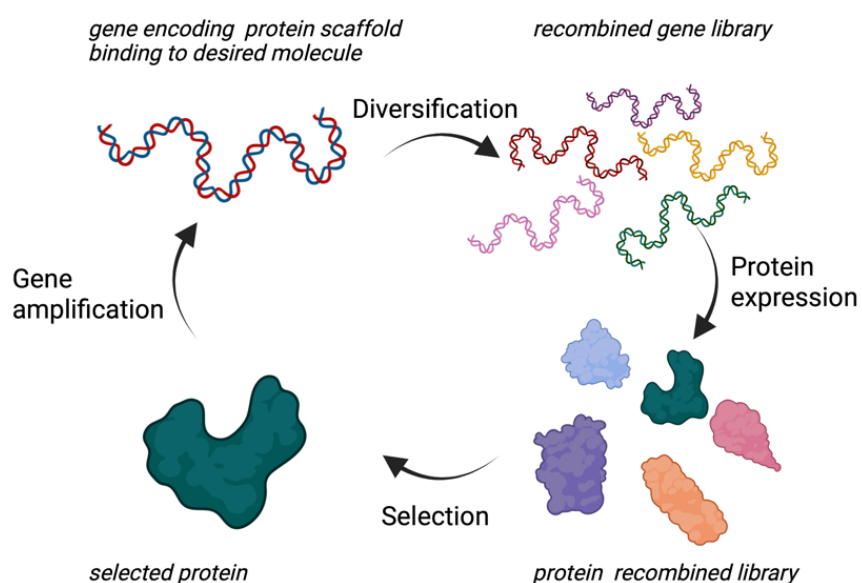
Figure 1: Diagram of directed molecular evolution of proteins (created by BioRender.com,2023; based on Matsuura et al. 2006)

3.4.1 Diverse DNA library generation

Diversification of the DNA encoding the protein of interest is performed by mutation of determined part of DNA by random mutagenesis or recombination (Mate *et al*. 2017). Several demonstrative methods of DNA library diversification are presented in the chapter 3.3.1.1.

3.4.1.1 Random mutagenesis methods

3.4.1.1.1 Error-prone PCR

Error-prone PCR (ep-PCR) is robust and simple technique used in direct evolution for creating random mutations in specified section of the DNA. The borders of the mutated region can be defined by appropriately chosen primers. Principle of random mutagenesis of the ep-PCR comes from of the suppression of the 3′ to 5′ exonuclease activity of the Taq polymerase (Ji & Day 2020), which can be even more suppressed by the Mg^{2+} ions in the reaction (Wilson & Keefe 2001).

In balanced amount, Mg^{2+} ions coordinate α-phosphate of deoxynucleotide (dNTP), facilitates the β-phosphate and γ-phosphate removal, which assist to nucleophile attack of 3'-OH on dNTP and phosphodiester bond formation (Yang *et al.* 2004). Mg^{2+} ions also influence melting temperature by binding to negative phosphate charge of DNA and decreasing of electrostatic repulsive forces between DNA strands. This contributes to correct and specific annealing of the primers to the DNA template strand. An excess of Mg^{2+} ions can lead to toleration of nonspecific affinity of primer to the template DNA strand (Lorenz 2012), increasing the likelihood that it will misread or skip nucleotides during replication (www.excedr.com, 2023, online).

Thus, random mutations can be inserted into DNA during the polymerase chain reaction (PCR). In directed evolution, the recommended number of mutated amino acids per gene is 1-4 (Wong *et al.* 2006). The mutation frequency of ep-PCR can be controlled with number of cycles of the PCR (Wilson & Keefe 2001) and by the concentration of the DNA template used in the reaction according to commercial protocol (Genemorph II Mutagenesis Kit protocol, Agilent Technologies, USA). Ep-PCR is one of the most widely used techniques for DNA diversification (Mate *et al.* 2017) and it can be applied for selection of improved proteins to increase affinity to its ligand, solubility, and folding stability (McCullum *et al.* 2010). Some disadvantages of ep-PCR include transitional mutation formation tendency created by polymerase used in ep-PCR or "hot spot" places on DNA chain, which mean positions of nucleotides with higher mutation frequency (Rogozin & Pavlov 2003). Some commercial kits (for example GeneMorph II) provide a combination of DNA polymerase Mutazyme I and Taq polymerase mutant enzymes to help minimize the tendency for transient mutations (Mate *et al.* 2017). Random mutagenesis method eliminating mentioned disadvantages of ep-PCR is Sequence Saturation mutagenesis (SeSaM) (Ruff *et al.* 2014). Diagram of recombinant DNA library construction via ep-PCR is shown in Figure 2.

Figure 2: Constructing a recombinant DNA library in directed evolution process via ep-PCR (created by BioRender.com, 2023)

3.4.1.1.2 Sequence saturation mutagenesis

Sequence saturation mutagenesis (SeSaM) is technique including 4 steps. In the first part, using a mixture of dNTPs containing phosphothioate-modified and standard bases, PCR can be used to generate ssDNA molecules of varying lengths. It's because of thioate-modified bases that are randomly incorporated into the newly formed ssDNA strands during this process (Mate *et al.* 2017). Subsequently, these phosphothioester bonds can be cleaved by iodine under alkaline conditions. Additionally, as a biotin-labelled forward primer was ingested during PCR, the 5' end of the ssDNA can be biotinylated, enabling its separation using streptavidin (Wong *et al.* 2004). In step 2, terminal deoxynucleotidyl transferase is used to add a universal base analogue to the 3' end of separated ssDNA fragments to "tail" them. In step 3, the "tailed" fragments are extended to full length using an ssDNA template. In step 4, the nucleotide analogues in the amplicons are randomly replaced by standard nucleotides during final PCR, resulting in dsDNA (Ruff *et al.* 2014).

3.4.1.1.3 PCR site directed mutagenesis

PCR site directed mutagenesis is method that enables the change of protein amino acid sequence by point mutation of DNA encoding it (Edelheit *et al.* 2009). This is achieved by DNA primer design for PCR that contains changed base in the appropriate codon so that this codon encodes the desired amino acid. For the primer to fit well even with the changed base, it is advisable that it contains at least 10 additional complementary positions from the changed base on each side (Bachman 2013). Then, the parental DNA is removed by methylation-dependent endonuclease enzyme (DnpI), so hemimethylated DNA containing mutation can be separated (Bachman 2013; www.adgeneblog.com, 2023, online).

3.4.1.1.4 Cassette mutagenesis

Cassette mutagenesis is a form of site-directed mutagenesis that exchanges a fragment of target DNA with a short, double-stranded oligonucleotide sequence (gene cassette). It works by using complementary restriction enzyme digest ends on the target DNA and gene cassette that can contain multiple mutations (Worrall 1994).

3.4.1.2 Recombination methods

3.4.1.2.1 DNA shuffling

In the first step of DNA shuffling, parental DNA from two different templates is randomly digested by DNase I. After that, fragments of the required size can be isolated by agarose electrophoresis and then randomized and extended by polymerase during PCR under appropriate set conditions. Randomization is possible when annealing fragments from different

parental DNAs are highly similar (Joern 2003). According to a recent study, DNA shuffling can lead to development of an enzyme with improved thermostability and fibrinogen hydrolytic activity (Yao *et al.* 2022).

3.4.1.2.2 Staggered extension process

Staggered extension process (StEP) is method used for recombination of different template parental DNA with approximately 80% identity during appropriately PCR set conditions (Zhao 2004). Principle of StEP consists in interrupting of the extension of the partly extended primer by polymerase. Then, partly extended primers are denatured and randomly hybridized to templates (Aguinaldo & Arnold, 2003). This process of extension interruption, denaturation of incompletely extended fragments, random hybridization and another extension is repeated due to required recombination frequency, or until the full-size fragments are formed (Mate *et al.* 2017; Zhao 2004).

3.4.2 Display-selection techniques

Display selection techniques are methods presenting the connection between genotype and phenotype by the entity that displays the nascent protein molecule and holds its encoding DNA or RNA sequence (genotype) at the same time. Thus, a physical connection is formed between the protein molecule's properties (phenotype) and its encoding sequence (Karatan *et al*. 2005). This approach can be used for seeking the DNA encoding protein variants that specifically binds with molecular target. Typical sizes of displayed libraries and commonly used organism in specific type of display selection technique are summarized in Table 2.

Table 2: Typical sizes of displayed libraries and commonly used organism in specific type of display selection technique

Type of display-selection technique	Typical library size	Commonly used organism	Literature
Phage display	10^{10} - 10^{12}	bacteriophage T7, bacteriophage M13, bacteriophage λ	Smith *et al.* 2015; Wang and Liu 2014; Karatan *et al.* 2015
Bacterial display	10^8 - 10^{10}	*E. coli, B. subtilis, L. bacillus*	
Yeast display	10^6 – 10^7	*S. cerevisiae, P. pastoris*	
Ribosome display	10^{12} - 10^{14}	*E. coli*	Plückthun *et al.* 2012; Karatan *et al.* 2005
mRNA display	10^{12} - 10^{14}	*E. coli*	Cotten *et al.* 2012; Karatan *et al.* 2005

3.4.2.1 Phage display

Phage display is technique used for studying interactions between protein and another protein/polypeptide, or nucleic acid using the bacteriophage surface. To display the encoded information at the surface of the virion with desired properties, the DNA coding the protein for displaying is inserted into the sequence of coat protein of the bacteriophage (Karatan *et al.* 2005). Then, by several rounds of affinity selection of bound peptides to its target called biopanning (Smith & Petrenko 1997), the proteins with inserted fragment recognized by specific antibodies can be separated (Sheenan & Marasco 2015). The most frequently used bacteriophages for phage display included bacteriophage M13, bacteriophage T7 and bacteriophage λ (Ebrahimizadeh & Rajabibazl 2014).

3.4.2.2 Cell surface display

Cell surface techniques enable to display expressed proteins or polypeptides into the surface of the cell. Main advantage of this method is that it is easy to detect and separate the required cells using fluorescence-activated cell sorting (FACS) by flow cytometer. Another benefit of cell surface display method is relatively inert surface of carbohydrates for non-specifically target protein binding (www.creative-biolabs.com, 2022, online; Karatan *et al.* 2005). Depending on whether the prokaryotic or eukaryotic cells are used for displaying, cell surface display methods can be divided into two branches – bacterial display and yeast display (Karatan *et al.* 2005).

3.4.2.2.1 Yeast display

Yeast display is versatile method extensively used in protein engineering for protein-scaffolds affinity studies (Boder & Wittrup 1997). The most common type of yeast used for yeast display is Saccharomyces cerevisiae (Tanaka & Kondo 2015). Yeast display technique uses possibility of displaying protein scaffold via C-terminal fusion with α-agglutinin protein subunit 2 (Aga2p). Fused Aga2p-protein scaffold is bound by two disulfide bonds to α-agglutinin protein subunit 1 (Aga1p), which is linked to the yeast cell surface by β-glycan bond (Zahradnik *et al.* 2021). Such fused protein scaffold can react with desired protein target. Because of C-terminal fluorescent tagged protein scaffold, it is possible to determinate cells expressing clones containing recombinant part - the protein scaffold. Specific target of scaffold derived binders is labeled by another fluorescent antibody and once the fluorescently tagged protein target is bound to protein scaffold, it is possible to sort the cells with double fluorescence signal by FACS (Stern *et al.* 2020; Karatan *et al.* 2005).

3.4.2.2.2 Bacterial display

Bacterial display is technique that can put on view a short polypeptide translocated from the cytoplasm (where it was expressed) of the bacteria into the bacteria surface (Lee *et al.* 2006). Thus, displayed libraries can be selected using FACS or biopanning selection procedures for affinity to protein target studies. The most used bacteria strains for bacterial display are *Escherichia coli* and *Staphylococcus aureus* (Karatan *et al.* 2005).

3.4.2.3 *In vitro* display

In vitro display methods are cell free techniques, offering possibility of phenotype coupling genotype *in vitro* without a limitation of cell surfacing. They can be divided into two similar types of methods: Ribosome display and mRNA display (Karatan *et al.* 2005).

3.4.2.3.1 Ribosome display

Ribosome display is method based on one-step *in vitro* translation and transcription of the linear DNA template leading to stable mRNA-ribosome-protein complex establishment (Zahnd *et al.* 2007) due to absence of stop codon in the encoding DNA. DNA construct for ribosome display should contain elements for *in vitro* transcription and translation - T7 promotor, ribosome binding site and TolA linker for regular exposure of the incipient synthetized protein scaffold. TolA linker is domain standardly used in ribosome display. Nascent protein could be then folded and presented in its full-length to its desired target reactive form (Plückthun 2012). When the ribosome complex is exposed to the target, the emerging protein variants binding the target can be selected by its affinity to the target, whereas the other variants can be washed out. Then using an EDTA solution to disrupt the ribosomes for releasing the mRNA, reverse transcription to re-write mRNA into ssDNA, we can obtain DNA library of high affinity clones to their molecular target (Karatan *et al.* 2005).

3.4.2.3.2 mRNA display

Technique called mRNA display is very closely related to ribosome display, except for the newly synthetized polypeptide chain is covalently bound to the structure of puromycin that substitutes the 3'end of tyrosyl t-RNA during translation, whereas the ribosome is released from the mRNA (Karatan *et al.* 2005; Newton *et al.* 2020). Scheme of ribosome display selection method is depicted in Figure 3.
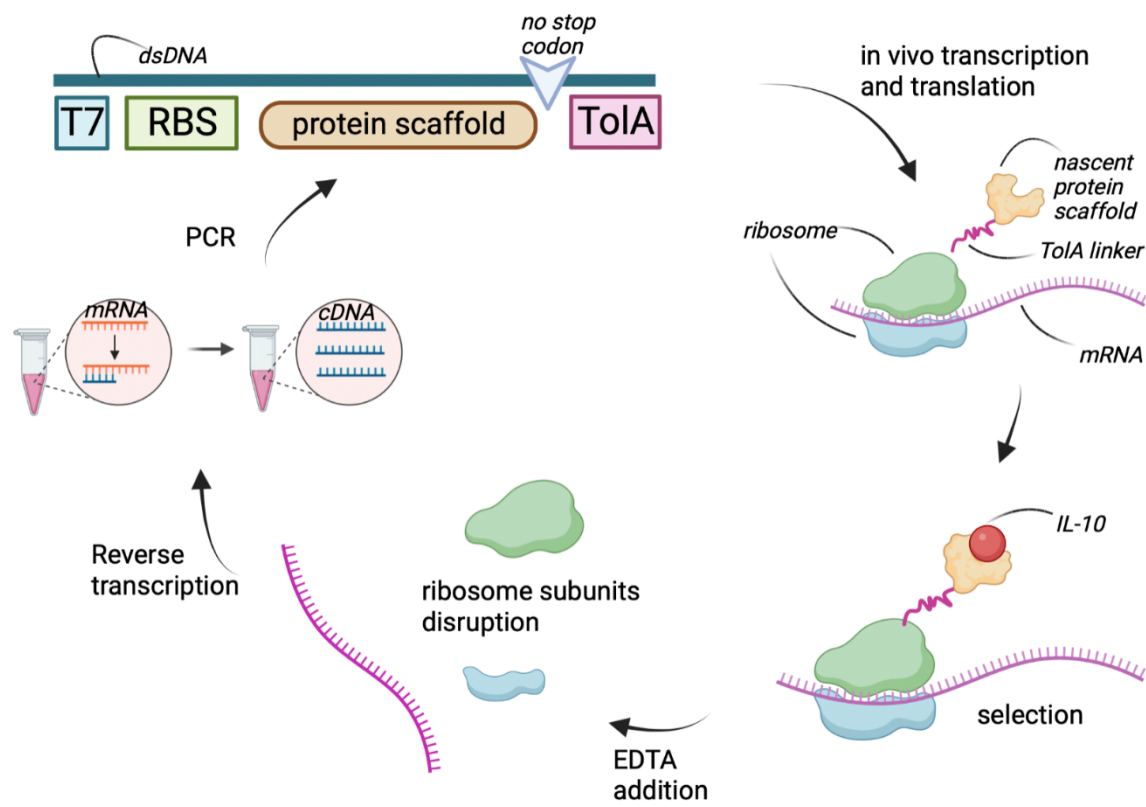
Figure 3: Scheme of ribosome display selection method (created by BioRender.com, 2023)
T7: T7 promotor; RBS: ribosome binding site; TolA: TolA linker.

4 Experimental part

4.1 Material and equipment

4.1.1 Chemicals

1-Step Turbo TMB-ELISA	-	Biowest (France)
Acetic acid	-	Sigma-Aldrich (Germany)
Acrylamide	-	PanReac AppliChem (Germany)
Agarose	-	Peqlab Biotechnologie GmbH (Spain)
Amino acids	-	RTSTM 100 *E. Coli* HY Kit Biotech rabbit (Germany)
Ammonium persulfate (APS)	-	Sigma-Aldrich (Germany)
B-PER™ Bacterial Protein Extraction Reagent	-	Thermo scientific (USA)
Blasticidin	-	Invivogen (France)
Bromphenol blue	-	Sigma- Aldrich (Austria)
BXT buffer solution	-	IBT lifesciences (Germany)
Calcium chloride (CaCl$_2$)	-	Lach-ner (Czech Republic)
Ciprofloxacin	-	Sigma-Aldrich (Germany)
Coomassie Brilliant Blue G-250	-	Sigma-Aldrich (England)
Coomassie Brilliant Blue R-250	-	Sigma-Aldrich (England)
CutSmart® Buffer	-	New England BioLabs (USA)
Diethyl pyrocarbonate (DEPC)	-	Sigma-Aldrich (Germany)
Dimethyl sulfoxide (DMSO)	-	Thermofischer scientific (France)
diSodium carbonate (Na$_2$CO$_3$)	-	Sigma-Aldrich (Germany)
dNTP mix	-	GeneMorph II Random mutagenesis kit (USA)
dNTP mix	-	Thermo scientific (USA)
Edetic acid (EDTA)	-	Lach-ner (Czech Republic)
Effectene Transfection Reagent	-	QIAGEN (Germany)
Ethanol 96% (EtOH)	-	Penta (Czech Republic)
GelRed®	-	Sigma-Aldrich (Germany)
Glycerol	-	Penta (Czech Republic)
Goat pAb to c-Myc (HRP)	-	Abcam (England)
GoScript™ 5X Reaction Buffer	-	GoScript™ Reverse Transcription System (USA)

Heparin	-	Sigma-Aldrich (Germany)
Hydrogen chloride 35% (HCl)	-	VWR (France)
Imidazol	-	Alfa Aesar (Germany)
Insect-XPRESS™ Protein-free Insect Cell Medium	-	Lonza (Belgium)
Izopropyl β-D-1-tiogalaktopyranozid (IPTG)	-	Formedium (Netherlands)
Kanamycin	-	Serva (Germany)
Luria-Bertani agar (LB agar)	-	Formedium (England)
Luria-Bertani broth (LB broth)	-	Formedium (England)
Magnesium di(acetate) (MgAc)	-	Sigma-Aldrich (Japan)
Mercaptoethanol	-	Sigma-Aldrich (Germany)
Methionine	-	RTSTM 100 E. Coli HY Kit Biotech rabbit (Germany)
Mutazyme II reaction buffer	-	GeneMorph II Random mutagenesis kit (Aligent, USA)
Nickel sulfate (NiSO4)	-	Sigma-Aldrich (USA)
PCR Nucleotide Mix	-	GoScript™ Reverse Transcription System (USA)
Phosphate buffer solution (PBS)	-	Institute of biotechnology (Czech Republic)
Pierce Protein free blocking buffer	-	Thermo scientific (USA)
Pulronic F-127	-	Thermo scientific (USA)
Purple loading dye	-	Thermo scientific (Lithuania)
Q5 reagent buffer	-	New England BioLabs (USA)
Reaction mix	-	RTSTM 100 E. Coli HY Kit Biotech rabbit (Germany)
Recombinant RNasin® Ribonuclease Inhibitor (RNasin 1)	-	GoScript™ Reverse Transcription System (USA)
Reconstruction buffer	-	RTSTM 100 E. Coli HY Kit, Biotech rabbit (Germany)
Ribolock RNase inhibitor (RNasin 2)	-	Thermofischer scientific (Lithuania)
Sodium chloride (NaCl)	-	Penta (Czech Republic)
Sodium dodecyl sulfate (SDS)	-	Sigma-Aldrich (China)
Sodium hydroxide (NaOH)	-	Lach-ner (Czech Republic)

Sodiumhydrogen carbonate (NaHCO3)	-	Sigma-Aldrich (France)
Strep-Tactin®XT 4Flow® high-capacity resin	-	VWR (Germany)
Superdex® 200 10/300GL	-	GE Healthcare (Sweden)
T4 buffer	-	New England BioLabs (USA)
Tetramethylethylendiamin (TEMED)	-	Sigma-Aldrich (China)
Trisaminomethane (Tris)	-	Sigma-Aldrich (USA)

4.1.2 Instruments and equipment

Agarose electrophoresis equipment	-	Bio-Rad (USA)
Centrifuge Alegra X-30R	-	Beckman Coulter (USA)
Centrifuge Avanti JXN-30	-	Beckman Coulter (USA)
Chromatography system	-	Bio-Rad (USA)
Clariostar Microplate Reader	-	BMG LABTECH (Germany)
CO_2 Incubator NB 203C	-	N-Biotek (South Korea)
Column with Streptactin XT matrix	-	Iba-lifesciences (Germany)
Concentrator VIVASPIN 2	-	Sartorius (UK)
DNA/RNA UV cleaner BOX, UVT-S-AR	-	BIOSAN (Latvia)
DS-11nanodrop Spectrophotometer	-	Denovix (USA)
EVE automatic cell counter	-	NanoEnTek (USA)
EVE cell counting slide	-	NanoEnTek (USA)
Flow box safe-fast-classic	-	Scholler (Italy)
His-trapTM	-	Cytiva (Germany)
INNOVA 44 incubator shaker series	-	Eppendorf (Germany)
Inverse microscope Eclipse TS100	-	Nikon (China)
Minicentrifuge Microcentrifuge 20	-	Beckman Coulter
Monolith NT.115	-	NanoTemper (Germany)
Monolith NT.115™ Standard Treated Capillaries	-	NanoTemper (Germany)
pH meter Orion star A211	-	Thermo Scientific (USA)
SDS electrophoresis equipment	-	Bio-Rad (USA)
Shaker IKA RCT basic	-	Sigma-Aldrich (USA)
Shaking incubator NB205	-	N-Biotek (South Korea)
SnapGene software	-	Dotmatics (USA)

Sonicator	-	Q Sonica, Thermo scientific (USA)
Stirring water bath	-	Major science (Taiwan)
Strep-Tactin®XT 4Flow® high-capacity resin	-	VWR (Germany)
Superdex® 200 10/300GL	-	GE Healthcare (Sweden)
Thermoblock	-	Bioer (China)
Thermocycler PCR system	-	Thermo Scientific (USA)
Ultrospec 10, cell density meter	-	Amersham biosciences (UK)
Vortex	-	Biosan (Latvia)

4.1.3 Plasmids

pCoBlast	-	Thermo Scientific (USA)
PETsm	-	Thermo Scientific (USA)
pMTH-BiP-IL10-Chis	-	Thermo Scientific (USA)
pRDVsm	-	Thermo Scientific (USA)

4.1.4 Primers

$4PSF_{for}$ primer $(5´ \rightarrow 3´)$ -   Thermo Scientific (USA)
AAGTCCATGGCACAGGGACCCGGG

$4PSF_{rev}$ primer $(5´ \rightarrow 3´)$ -   Thermo Scientific (USA)
GTTCGGATCCGATGGAGCCCATGAATG

$T7B_{fw}$ primer $(5´ \rightarrow 3´)$ -   Thermo Scientific (USA)
ATACGAAATTAATACGACTCACTATAGGGAGACCACAACGG

$TolAk_{rev}$ primer $(5´ \rightarrow 3´)$ -   Thermo Scientific (USA)
CCGCACACCAGTAAGGTGTGCGGTTTCAGTTGCCGCTTTCTTTCT

pETup 2 primer $(5´ \rightarrow 3´)$ -   Thermo Scientific (USA)
GATGCGTCCGGCGTAGAGG

4.1.5 Cells

E. coli BL21(DE3) Gold chemically competent cells	-	Thermo Scientific (USA)
E. coli TOP10 chemically competent cells	-	Thermo Scientific (USA)
Schneider 2 cells	-	Thermo Scientific (USA)

4.1.6 Enzymes

BamHI-HF	-	New England BioLabs (USA)
Q5 DNA polymerase	-	New England BioLabs (USA)
GoScript™ Reverse Transcriptase	-	GoScript™ Reverse Transcription System (USA)
Mutazyme II DNA polymerase	-	GeneMorph II Random mutagenesis kit (Aligent, USA)
NcoI-HF	-	New England BioLabs (USA)
T4 ligase	-	New England BioLabs (USA)

4.1.7 Markers

DNA low range Ladder	-	Thermo scientific (Lithuania)
SDS-PAGE protein mass standard	-	Thermo scientific (Lithuania)

4.1.8 Biological material

Bovine serum albumine (BSA)	-	Sigma-Aldrich (Germany)
E. coli lysate	-	RTSTM 100 E. Coli HY Kit, Biotech rabbit (Germany)
Fetal bovine serum (FBS)	-	Gibco (USA)
S. cerevisiae RNA	-	RTSTM 100 E. Coli HY Kit, Biotech rabbit (Germany)

4.1.9 Commercial kits

Effectene Transfection Reagent	-	QIAGEN (Netherlands)
GeneMorph II Random mutagenesis kit	-	Aligent (USA)
High pure RNA isolation Kit	-	Roche life science (Germany)
Monolith protein labeling kit red-tris-Nta	-	NanoTemper (Germany)
NucleoBond Xtra Midi EF, Midi kit Endotoxin-free plasmid DNA	-	Machery-Nagel (Germany)
NucleoSpin Gel and PCR Clean-up	-	Machery-Nagel (Germany)
Plasmid purification, Miniprep kit-I, peqGOLD	-	VWR (Germany)
RTSTM 100 E. Coli HY Kit	-	Biotech rabbit (Germany)

4.1.10 Buffers and solutions

IL-10 purification via NiNTA affinity chromatography

- Supernatant buffer: 50 mM $CaCl_2$; 10 mM $NiSo4$; 2M NaCl; 500 mM Tris, pH 8.0, filtered
- Equilibration buffer: 50 mM Tris, pH 8.0; 300 mM NaCl, filtered
- Elution buffer: 50 mM Tris, pH 8; 300 mM NaCl; 250 mM Imidazole, filtered

Size Exclusion Chromatography

- Equilibration buffer: 50 mM Tris, pH 8.0; 300 mM NaCl, filtered

Ribosome display

- 0.1% DEPC water: 1 ml of DEPC diluted in Milli Q water, placed into incubator for 2 hours at 37°C, then autoclaved
- Bicarbonate coating buffer: 0.303 g of Na_2CO_3 and 0.6 g of $NaHCO_3$ diluted in 0.1% DEPC water, pH adjusted to 9.6, filled into final volume 100 ml with 0.1% DEPC water, filtered
- TBS buffer: 1.21 g of Tris and 1.75 g of NaCl diluted in 0.1% DEPC water, pH adjusted to 7.5 with HCl, filled into 200 ml volume with 0.1% DEPC water, autoclaved
- WBT buffer: 1.21 g of Tris, 1.75 g of NaCl and 2.14 g of MgAc diluted in 0.1% DEPC water, pH adjusted to 7.5 by acetic acid, volume filled in to 200 ml with 0.1% DEPC water, filtered
- EB (elution) buffer: 1.21 g of Tris, 1.75 g of NaCl and 2.92 g of EDTA diluted in 0.1 DEPC water, pH adjusted to 7.5 by acetic acid and filled into volume 200 ml with 0.1%DEPC water, filtered
- Frozen reaction mix: 12 µl of *E. coli* lysate, 10 µl of Reaction mix, 12 µl of amino acids, 1 µl of Methionine and 5 µl of reconstitution buffer, mixed and stored at -20°C (all from commercial kit RTSTM 100 E. Coli HY Kit, Biotech rabbit, (Germany)).
- WBT mix: 410 µl of WBT buffer mixed with 83 µl of 3% BSA (in PBS) and 6.25 µl of 200 mg/ml heparin solution.
- Elution solution: 1 ml of EB buffer mixed with 50 µl of *S. Cerevisiae* RNA (1 mg/ml) and 12.5 µl of Heparin (200 mg/ml).

SDS-PAGE

- Sample buffer (5x concentrated): 2 g of SDS and 0.01 g of Bromphenol blue diluted in 10 ml of glycerol, 6 ml of 1 M Tris (pH 6.8) and filled into volume of 20 ml with dH_2O. Into 475 µl of sample buffer, 25 µl of β-mercaptoethanol was added.
- Staining solution: 0.05 g of Coomassie Brilliant Blue G-250 and R-250 diluted in dH_2O and 1.5 ml of acetic acid, filled into volume 500 ml and filtered through paper filter

- Tank buffer: 6.07 g of Tris, 28.82 g of glycine and 20 g of SDS diluted and filled up to volume 2 l with dH$_2$O.

Agarose electrophoresis

- TAE buffer: 4,84 g of Tris, 1.14 ml, and 2 ml 0.5 M NaOH diluted and filled into volume of 1 l with dH$_2$O.

- 1% agarose gel: 1.5 g of agarose diluted up to volume of 150 ml by TAE buffer

4.1.11 Biological material

Bovine serum albumin (BSA)	-	Sigma-Aldrich (Germany)
S. cerevisiae RNA	-	Thermo scientific (Lithuania)
Fetal bovine serum (FBS)	-	Gibco (USA)

4.2 Methods

4.2.1 IL-10 production by S2 cells

4.2.1.1 Thawing of the S2 cells frozen stock

The principles ensuring maximum sterility in the antiseptic environment of the flowbox were followed throughout the handling of the cell cultures for the entire time. An Eppendorf tube containing S2 cell line, which is derived from Drosophila melanogaster embryos, was transferred into a water-bath heated to 37 °C for five min. After that, cells were transferred into a 15ml tube containing 7 ml of fresh growth medium (Insect-Xpress) with 15 % FBS and centrifuged at 1000 x g for three min. Then, the supernatant was discarded, and the pellet was resuspended by pipetting. After that, 1 ml of fresh complete growth medium (X-Press Insect Medium with ciprofloxacin) with 15 % FBS and resuspended cells was transferred into one well of a 12-well plate. Finally, this plate was placed into a 27 °C heated thermobox.

4.2.1.2 Passaging of the S2 cells

By passaging of the cells, it is meant the transfer of them into fresh X-Press Insect Medium containing ciprofloxacin for propagation of a cell line and incubation in a 27 °C warmed thermobox for optimal growth conditions. To obtain stable cell line culture during passaging and gradual increasing of the culture volume, two rules were followed. The first rule was that before every medium addition, cells were counted using an automatic cell counter and Tryptan blue dye: 10 µl of cell culture was diluted into 10 µl of dye which caused living cells not to take up the dye whereas dead cells did; this enabled counting both living and dead cells. The second rule stated that the amount of living cells must not be reduced to less than one million per milliliter based on their previous count.

4.2.1.3 Transfection of pMTH-BiP-IL10-Chris plasmid into S2 cells

Approximately 15 ml of stable, regular-shaped line cell culture with no apoptosis corpuscles seen under 40x magnification by an inverted microscope, 97 % viability and 1×10^7 cells/ml concentration were obtained by passaging as described in the previous paragraph. This cell culture was dosed at 1.5 ml into five wells of a 24-well plate. Then, 0.5 ml of the culture from each of the previous five wells was diluted in 0.5 ml of fresh X-press insect medium and distributed into five new wells. The cells were grown overnight in a 27 °C heated thermobox until optimal cell confluence of around 90 % was reached. The next day, two wells with optimal cell confluence were chosen for transfection using commercial transfection kit Effectene Transfection Reagent (ETR kit).

33

From each well containing 1 ml of culture, 0.4 ml of medium was discarded. Then, a transfection reagent was prepared in a 1.5 ml plastic tube by mixing 60 µl of EC buffer (from ETR kit), 20 ng of pCoBlast plasmid, 200 ng of pMTH-BiP-IL10-Chris plasmid and 1.6 µl (from ETR kit). The transfection reagent tube was vortexed and incubated at room temperature for 5 min. Next, 6 µl Effectene reagent were added to the transfection reagent tube; it was mixed 5x by pipetting and incubated for 10 min at room temperature to allow formation of the transfection complex. After that, 0.4 ml of fresh complete growth medium was added to the transfection reagent tube; it was mixed by pipetting and immediately added gently into the chosen plate wells with cell culture using dripping-pipetting technique. Finally, the plate was placed into a 27°C heated thermobox.

Next morning, the medium was carefully pipetted from the wells to prevent resuspendation of cells from the bottom of the wells and replaced with fresh growth medium containing 15% FBS. It was then incubated for 2 days in a 27 °C heated thermobox. After two days, the cells were passaged by adding complete growth medium containing 12 µl of Blasticidin S (10 mg/ml) to 2 ml of cell culture volume.

After two days, the cells had a regular shape with no apoptotic corpuscles outside of them, as seen through an inverted microscope (Eclipse TS100) at 40x magnification. The concentration of living cells reached up to 0.7×10^7 cells/ml and viability was determined as 96 %. Cells were diluted by 2 ml of complete fresh-grown medium with 15 % FBS to a total volume of 4 ml, and 12 µl of Blasticidin S was added. Cell culture was transferred into a sterile 50 ml flask and placed in a 27 °C heated thermobox for two days. After two days, cells were checked using an inverted microscope to ensure that transfection had gone well, and only stable transfected cells were selected. After that, cell concentration was measured (via automatic cell counter and trypan blue solution usage) and then, the cell culture was diluted to 8 ml with fresh complete growth medium, so a concentration of 1.1×10^6 cells/ml was obtained. The diluted cell culture was transferred into a sterile 50 ml shake cultivation flask and placed in a shaking incubator heated at 27 °C. The volume of the complete growth medium addition, based on concentration determination via an automatic cell counter and trypan blue solution usage, was gradually increased into the cell culture for a stable line to obtain protein production. The cell doubling time was approximately 2-3 days.

After 29 days, 1 liter of regular-shaped cells with no apoptosis corpuscles visible under an inverted microscope at 40x magnification and a concentration of 1×10^7 and viability of 98 % was obtained. The cells were induced by 1 mM $CuSO_4$, transferred into two 2 l shake cultivation flasks, and shaken for 5 days in a 27 °C heated thermobox. In the next step, cell culture was centrifuged at 4500 x g, 10 °C for 30 min. The supernatant containing secreted IL-

10 was kept at -80 °C. Of the 950 ml of supernatant, 400 ml was intended for purification via affinity chromatography and size exclusion chromatography; 550 ml of the remaining supernatant was stored at -80 °C.

4.2.1.4 IL-10 purification via affinity chromatography

400 ml of thawed supernatant with secreted IL-10 was buffered by 40 ml of buffer solution (50 mM $CaCl_2$; 10 mM $NiSO_4$; 2 M NaCl and 500 mM Tris, pH 8.0) and stirred for 1 hour at room temperature. Then, buffered supernatant was centrifuged at 5000 x g, 4 °C for 15 min and then filtered by vacuum filtration apparatus.

His-trap^{TM} column was washed by distilled water and by wash buffer (300 mM NaCl; 50 mM Tris, pH 8.0). Then, the protein sample was eluted by elution buffer solution (300 mM NaCl; 50 mM Tris, pH 8.0; 500 mM Imidazole). Elution fractions were collected into the prepared 1.5 ml sterile micro plastic tubes.

4.2.1.5 Concentration of IL-10

Fractions 34-42 obtained via affinity chromatography (depicted in Figure 5) were concentrated via Vivaspin centrifugal concentrator with 10 kDa size pores of a polyether sulfone membrane. The sample was loaded into the membrane and centrifuged at 6000 x g, 10 °C until the volume of sample above the membrane reached 0.5 ml.

4.2.1.6 Size exclusion chromatography purification of IL-10

For size exclusion chromatography purification, Superdex column was used. First, the column was washed by filtered dH_2O and equilibrated by equilibration buffer (50 mM Tris, pH 8.0; 300 mM NaCl). Also, the injection loop was washed by the same equilibration buffer solution. Column flow was set on 5 ml/min and the protein sample was injected into the injection valve. Purified protein fractions were collected into the prepared sterile 1.5 ml plastic tubes. In the final step, column was washed by filtered dH_2O and 20% filtered ethanol for column storage.

4.2.1.7 SDS-PAGE of purified IL-10

The purity of fractions 13-15 and 18-20 were verified through SDS-PAGE. The solution of the mixture for 1 polyacrylamide gel is listed in Table 3.

Table 3: Solution of 15% polyacrylamide gel

Polyacrylamid gel component	Volume of running gel	Volume of stacking gel
dH_2O	0.55 ml	1.23 ml
Acrylamid 30 %	2.5 ml	266 µl
Tris 1 M pH 8.8	1.87 ml	200 µl
SDS 10 %	50 µl	60 µl
APS 25 %	12.5 µl	20 µl
TEMED	12.5 µl	5 µl

Into the 1.5 ml plastic tube, 8 µl of protein sample and 2 µl of sample buffer were added and placed into a 95 °C heated heatblock for 5 min. Then, the protein sample was centrifuged at 20,000 x g for 10 min. Into the gel wells, 5 µl of mass standard and 10 µl of protein sample were pipetted. In the next step, a source of direct voltage was set up to 220 V. Electrophoresis ran for 50 min, then the gel was washed with dH_2O, staining buffer solution, and decolored with an ethanol-water solution.

4.2.2 Transformation and isolation of required plasmids

4.2.2.1 Transformation of pMTH-BiP-IL10-Chris into chemically competent cells

DNA construct pMTH-BiP-IL10-Chris in volume of 1.4 µl was pipetted into 1.5 ml plastic Eppendorf tube with 50 µl of chemically competent TOP10 cells (melted at room temperature on ice) and left for next 25 min on ice. Then, the tube with cells and DNA construct was put into the thermobox warmed up to 42 °C for 45 seconds for heatshock. Tube was placed on ice immediately and left there for 3 min. After that, 750 µl of LB medium was pipetted into tube and shaken on 300 x g, 37 °C for 1 h. Then, the tube with grown cells was centrifuged at 4000 x g for 5 min. In the next step, supernatant was almost decanted, and pellet was resuspended by pipetting. Finally, the resuspended cells were plated on fresh agar plate with kanamycin antibiotic and placed overnight to 37°C.

4.2.2.2 Isolation and purification of plasmid DNA from transformed cells

Next morning, a single colony from agar plate was inoculated into 5 ml LB medium with kanamycin in 50 ml tube and shaken at 300 x g, 37°C for 8 h. 2 ml of this culture was pipetted into 200 ml LB with kanamycin in 1 l cultivation flask and shaken at 300 x g overnight in 37°C.

Isolation of plasmid DNA was performed according to manufacturer protocol (NucleoBond Xtra Midi EF, Midi kit for endotoxin-free plasmid DNA). Concentration of purified plasmid DNA is listed in Table A1 in appendix III.

4.2.2.3 Transformation and isolation of PRDVsm and PETsm plasmids

Transformation and isolation of TOP10 transformed cells with pRDVsm and pETsm constructs were done in the same way as described in selection 4.2.2.1 and 4.2.2.2 Concentrations of purified plasmid DNA is listed in Table A2 in appendix III.

4.2.3 Direct evolution of F5 and G3 clones derived from 57aBi protein scaffold

4.2.3.1 PCR of F5_WT and G3_WT clones

The primers were designed for the PCR to amplify the sequence of F5_WT or G3_WT clone (derived from 57aBi). PCR reaction is listed in Table 4, PCR reaction cycle is listed in Table 5.

Sequence of 4PSF$_{for}$ primer (5'→3'):   AAGTCCATGGCACAGGGACCCGGG

Sequence of 4PSF$_{rev}$ primer (5'→3'):   GTTCGGATCCGATGGAGCCCATGAATG

Table 4: Solutions or reaction component and order of their addition for PCR of clones F5 a G3

Order	Solution or reaction component	Volume [μl]
1	Milli Q water	30
2	Q5 buffer	10
3	dNTP	1
4	4PSFfor primer	2.5
5	4PSFrev primer	2.5
6	DNA template	2
7	DMSO	1
8	Q5 polymerase	1

Table 5: PCR setting for amplification of F5_WT and G3_WT clones

Cycle step	Temperature	Time	Number of
Initial	98	1 min	1
Denaturation	71	10 sec	
Annealing	72	45 sec	35
Extension	72	30 sec	
Final	72	5 min	1
extension	4	hold	

4.2.3.1.1 PCR product analysis via agarose gel electrophoresis with UV detection

Agarose solution (1% agarose in TAE solution) gel was heated up in a microwave oven, the gel was poured onto the tray placed in an electrophoretic bath. GelRed was used as an intercalating agent for UV detection. 12 µl of GelRed was pipetted dropwise into the gel tray and mixed gently. 5 µl of loading dye was pipetted into both samples after PCR. The source of voltage was set to 120 V. After removing the comb, 10 µl of marker was pipetted into the solidified agarose gel and 25 µl from each sample with loading dye. After 25 mins, the gel was transferred under a UV source. After turning it on, DNA fragments of sample F5_WT and G3_WT were observed to distinguish, which approached from the wells to the positively charged anode, and which corresponded to the distance of the marker fragment of 406 bp.

4.2.3.1.2 Isolation of DNA from agarose gel

DNA fragments of the sample were excised from the agarose gel and the sections were then removed into a 1.5 ml Eppendorf plastic tube. Then the isolation of DNA was performed by commercial kit instructions (NucleoSpin Gel and PCR Clean-up). Concentrations of purified DNA fragments F5_WT and G3_WT are listed in Table A3 in appendix III.

4.2.3.2 Creation of diversified library derived from wild types via error-prone PCR

Clones F5_WT and G3_WT were amplified via Error-prone PCR used as an *in vitro* DNA diversification tool. We used the commercial kit (GeneMorph II Random Mutagenesis kit). The reaction composition was optimized and calculated for 1-4 nonsynonymous mutations per gene was aquired. Solution of reaction is listed in Table 6, PCR setting of parameters for reaction are listed in Table 7.

Analysis of error-prone PCR products via electrophoresis with UV detection and isolation of DNA was done in the same way as described on section 4.2.3.1.1 and 4.2.3.1.2 so DNA fragments of F5_EP and G3_EP were obtained.

Table 6: Solutions and order of their addition for error-prone PCR of clones F5_WT a G3_WT

Order	Solution	Volume [µl]
1.	Milli Q water	40
2.	Mutazyme II reaction buffer	5
3.	dNTP mix	1
4.	4PSF$_{for}$ primer	1
5.	4PSF$_{rev}$ primer	1
6.	DNA template	1
7.	Mutazyme II DNA polymerase	1

Table 7: Error-prone PCR setting program

Cycle step	Temperature [°C]	Time	Number of cycles
Initial denaturation	95	2 min	1
Denaturation	95	30 sec	30
Final extension	72	10 min	1

4.2.3.2.1 Restriction cleavage of F5_EP, G3_EP inserts and pRDVsm vector

Restriction cleavage solution for every single DNA template (pRDVsm plasmid/ F5_EP/G3_EP) is listed in Table 8. Once all 3 solutions were prepared, they were placed into 37°C heated thermobox overnight.

Table 8: Restriction cleavage solution for PRDVsm, F5_EP and G3_EP

Solution or reaction component	Volume [µl]
pRDVsm plasmid/ F5_EP/G3_EP	20
10 x Cut Smart buffer	3
MQ	5
NcoI	1
BamHI	1

Analysis of digested pRDVsm, F5_EP and G3_EP after restriction cleavage via electrophoresis with UV detection and DNA isolation using the commercial kit (NucleoSpin Gel and PCR Clean-up) was done in the same way as described in section 4.2.3.1.1 and 4.2.3.1.2.

4.2.3.2.2 Ligation of F5_EP and G3_EP inserts into pRDVsm plasmid

Ligation of cleaved inserts F5_EP and G3_EP into cleaved pRDVsm plasmid was performed. Ligation reaction solution is listed in Table 9.

Table 9: Ligation reaction solutions

Reaction component	Volume [µl]
Insert F5_EP / G3_EP	7
pRDVsm	10
10 x T4 buffer	2
T4 ligase	1

Once Ligation reactions were prepared, they were left in room temperature for 1 h. Then, the ligation mixture was stored in -20°C. Ligation plasmid products were named pRDVsm_F5 and pRDVsm_G3. Reaction was incubated for 1 h at room temperature, then stored in -20 °C.

4.2.3.2.3 Transformation of DNA constructs pRDVsm_F5/G3_EP into TOP 10 cells

Transformation was made in the same way as described in section 4.2.2.1, except for amount of DNA construct of pRDVsm_F5_EP and pRDVsm_G3_was 5 µl, which was pipetted into 50µl of chemically competent cells TOP10. The final culture was plated on 3 fresh agar plates (A, B, C for pRDVsm_F5_EP) and (D, E, F for pRDVsm_G3_EP) with kanamycin to be sure single colonies may be inoculated from next morning. 5 single colonies were inoculated from each agar plate with transformed constructs (pRDVsm_F5_EP / pRDVsm_G3_EP) into 2 ml of fresh LB medium with kanamycin and shaken at 180 x g, 37 °C overnight.

Next day, isolation of plasmid DNA contained diversified libraries after error-prone PCR, was performed by using the commercial kit (Plasmid purification, Plasmid Miniprep kit I). Concentrations of isolated plasmid DNA are shown in Table A4 in appendix III.

4.2.3.2.4 Sequencing of selected clones

As sequencing primer, pETup 2 primer was used. The amount of plasmid DNA was chosen to ensure that each 10 µl sequencing mix contained 7.5 µl of 100-200 ng of DNA and 2.5 µl of pETup2 primer. Samples were sent for sequencing to Eurofins company (Germany).

4.2.3.2.5 Sequence analysis

Results were analyzed through SnapGene program, then we transcripted DNA into amino acid sequence using online DNA-protein converter ExPASy translate tool (Gasteiger *et al*. 2003). Finally, we did multiple protein alignment of randomized clones, where original sequences of G3_WT and F5_WT clones were chosen as references. Using UGENE program (Okonechnikov *et al*. 2012), it was found out frequency and positions of mutations in protein phenotypes of our novel libraries generated by Error-prone method (see the Figure A2 in appendix II).

4.2.3.3 PCR of pRDVsm_F5_EP and pRDVsm_G3_EP

For ribosome display selection of products pRDVsm_F5_EP and pRDVsm_G3_EP products, PCR was proposed so final products contained transcription elements (T7 promotor), translation elements (ribosome binding site) and TolA linker for ribosome display. Solution of PCR reaction is listed in Table 10. PCR cycle is listed in Table 11. The arrangement of the ribosomal display construct can be seen in the Figure 3.

Table 10: Solutions and order of their addition for PCR PRDVsm_F5 and PRDVsm_G3

Order	Solution or reaction component	Volume [µl]
1	Milli Q water	29
2	Q5 buffer	10
3	dNTP	1
4	T7B$_{FW}$ primer	2.5
5	TolAk$_{rev}$ primer	2.5
6	DNA template (pRDVsm_F5_EP/G3_EP)	3
7	DMSO	1
8	Q5 polymerase	1

Table 11: PCR setting programe

Cycle step	Temperature [°C]	Time	Number of cycles
Initial denaturation	98	1 min	1
Denaturation	98	10 sec	
Annealing	72	30 sec	35
Extension	72	25 sec	
Final extension	72	4 min	1
	4	hold	

Analysis of PCR products via electrophoresis with UV detection and isolation of DNA was done in the same way as described in section 4.2.3.1.1 and 4.2.3.1.2. In the next step, isolation of DNA was done by using the commercial kit (NucleoSpin Gel and PCR Clean-up). Concentrations of obtained isolation products RD_F5$_{EP}$ and RD_G3$_{EP}$ are listed in Table A5 in appendix III.

4.2.3.4 Selection of IL-10 binding variants via ribosome display method

This method was performed according to Dr. Maros Huliciak´s protocol (Huliciak *et al*. 2023). Solutions of used buffers (WBT buffer, TBS buffer, EB buffer, Frozen reaction mix, bicarbonate coating buffer and WBT mix) is listed in chapter 4. 1. 10, Ribosome display paragraph.

IL-10 specific target and non-specific BSA immobilization

At the beginning, in microtitration plate, two locations of 4 wells (8 wells at all) were chosen: 1st location = preselection wells; 2nd location = selection wells.

Then, 100 ml of IL-10 (25 µg/ml, in bicarbonate coating buffer) was pipetted into each selection well and incubated at 4 °C overnight. Next day, 100 µl of Pierce protein free solution into each selection well and left for 1 hour at room temperature, to block possible hydrophobic interactions mediated by free plastic places. Then, selection wells were 3x washed by 300 µl of WBT buffer.

One-step translation and transcription

Frozen reaction mix in volume of 40 µl of was added into 10 µl of combinatorial library RD_F5$_{EP}$ (75.7 ng/µl) and RD_G3$_{EP}$ (79.3 ng/µl) and placed into thermocycler for 6 h at 30 °C and then at 4 °C overnight. Two eppendorf tubes containing 50 µl of translation/transcription mix for each clone (one for F5 and one for G3) were obtained. Then, into each tube with the mix, 200 µl of WBT mix was pipetted, and tubes were placed on ice for 1-2 min. Then, tubes were centrifuged at 14000 x g, 4°C for 5 min thereby tubes with translation complex were acquired.

Preselection (empty) wells were 3x washed with 300 µl of TBS and then they were filled with 300 µl of 3 % BSA (in TBS) at almost the same moment, the Pierce solution was added into selection wells as mentioned before. A microtitration plate was incubated then for 1hour in RT. Then, selection and preselection wells were washed 3x with WBT buffer.

Selection

Translation complex in volume of 110 µl was added into each of 2 preselection wells for each clone and shaken for 1hour at 4 °C. After that, supernatant from each well was transferred into selection well and incubated for 1 hour at 4 °C. Then, selection wells were 15 x washed according to the ribosome display round with WBT buffer.

Elution and purification of mRNA

Ice-cold elution buffer in volume of 100 µl was pipetted into each well and incubated for 1hour at 4 °C with shaking. After that, eluted mRNA was purified according to commercial kit and protocol from High pure RNA isolation Kit. In the end, aliquots of eluted mRNA for each clone were mixed (1 mix for F5 clone and 1 mix for G3 clone were obtained).

Reverse transcription

For reverse transcription, Solution 1 for each clone separately was made according to solution mix listed in Table 12. Then, obtained solution1_F5 and solution1_G3 were incubated at 65 °C for 5 min and then placed on ice for 2 min. After that, 25 µl of Solution2 was prepared by mixing solutions according to Table 13. 12.5 µl of Solution2 was pipetted into solution1_F5 and solution1_G3 and incubated for 1 hour at 42 °C.

Table 12:Solution mix for solution1_F5/solution1_G3

Order	Solution	Volume
1.	4PSF_rev primer	0.5
2.	dNTP mix	1
3.	eluted mRNA_F5/G3	11.5

Table 13: Solution2 mix

Order	Solution	Volume
1.	5x Reaction buffer	10
2.	RNasin1	0.5
3.	dNTP mix	10
4.	RNasin2	0.5
5.	DEPC water	2
6.	Reverse transcriptase	2

4.2.3.5 PCR amplification of cDNA ribosome display products

After reverse transcription reaction, obtained cDNA_F5 and cDNA_G3 fragments were amplified by PCR. The solution of reaction is listed in Table 14. The PCR setting program is listed in Table 15. Analysis of dsDNA PCR products named F5_sel and G3_sel via electrophoresis with UV detection was done in the same was as described in section 4.2.3.1.1, isolation of DNA was performed as described in section 4.2.3.1.2.

Table 14: Solutions and order of their addition for PCR cDNA_F5 and cDNA_G3.

Order	Solution	Volume [µl]
1.	Milli Q water	25
2.	Q5 buffer	10
3.	dNTP	3
4.	4PSF_rev primer	2.5
5.	4PSF_for primer	2.5
6.	cDNA template	5
7.	DMSO	1
8.	Q5 polymerase	1

Table 15: PCR setting programme

Cycle step	Temperature [°C]	Time	Number of
Initial denaturation	98	1 min	1
Denaturation	98	10 sec	
Annealing	66	45 sec	35
Extension	72	30 sec	
Final extension	72	5 min	1
	4	hold	

4.2.3.5.1 Restriction cleavage of pETsm/F5_sel/ G3_sel inserts and pETsm vector

Restriction cleavage solution for every single DNA template (pETsm/F5_sel/ G3_sel) is listed in Table 16. Once all 3 solutions were prepared, they were placed into 37°C heated thermobox overnight.

Table 16: Restriction cleavage reaction solutions

Name of reaction component	Volume [μl]
pETsm /F5_sel/ G3_sel	20
Cut Smart	3
MQ	5
NcoI	1
BamHI	1

4.2.3.5.2 Ligation into pETsm vectors

In the next step, ligation of cleaved F5_sel and G3_sel into cleaved pETsm plasmid was performed. Ligation reaction solution is listed in Table 17. Once ligation reactions were prepared, they were left in room temperature for 1 hour to complete the reaction.

Table 17: Ligation reaction solutions

Name of reaction component	Volume [μl]
Insert F5_sel/ G3_sel	7
pETsm	10
T4 buffer	2
T4 ligase	1

4.2.3.6 Transformation of pETsmF5_sel/G3_sel variants into BL21(DE3)-Gold cells

Transformation was made in the same way as described in section 4.2.2.1, apart from amount of used plasmid DNA. For this transformation, 5 μl of the ligation mixture was used. Ligation mixture was obtained as described in prevous paragraph. Final culture was plated on 3 fresh agar plates with kanamycin for each clone to ensure single colonies may be inoculated from next morning. Acquired transformation products were named petF5_sel and petG3_sel.

4.2.3.7 ELISA screening

Into each well of 96 deepwell (two deepwells in total) assigned to each clone of F5 and G3, 500 μl of LB medium with kanamycin was pipetted. Then, single colonies from agar plates with petF5_sel and petG3_sel cells were inoculated in to each well (192 inoculates of night culture was prepared at all). After that, both deepwells were shaken at 111 x g, 37°C overnight.

Next morning, 50 μl from every single well was pipetted into new microtitration plate with 15 % glycerol in the stock and stored in -80 °C.

In addition, 5 μl from each deepwell well of overnight culture was pipetted into new deepwell with 500 μl of fresh LB medium with kanamycin and shaked at 111 x g, 37°C for 4 hours. After 4 hours of cultivation, cultures were induced by 1 mM IPTG (in final concentration) and shaken at 18°C overnight.

Next morning, deepwells were centrifuged at 1000 x g at 4°C for 20 min and then the supernatant was discarded. Into each well, 100 μl of B-PER was pipetted for pellet resuspendation and cell lysate obtaining.

Microtitration plates were shaken at 360 x g in room temperature for 45 min and then, 100 μl of 3% BSA solution (BSA diluted in 50 mM Tris; pH 8.0, NaCl 300 mM buffer with 0.1 % Pulronic) was added into each well. Then, microtitration plates were and shaken then for 5 min at 360 x g in room temperature. Then, microtitration plates with overnight coated IL-10 (in each well was 100 μl of 50 μg/ml IL-10 diluted in bicarbonate coating buffer, coated in 4° C overnight) were blocked by 3 % BSA solution in room temperature for 2 hours. Then, microtitration plates were 3x washed by wash buffer (50 mM Tris, pH 8.0; 300 mM NaCl, 0.1 % Pulronic).

In the next step, 100 μl of cell lysate culture was pipetted into the microtitration plate (one plate for F5-WT derivate variants, another one for G3-WT derivate variants) into the corresponding position. Then, microtitration plates were shaken at room temperature for 1 hour and 3x washed by wash buffer. After that, into each microtitration plate well, 100 μl of 10 000x diluted antibody (Goat pAb to c-Myc) in 3 % BSA solution was pipetted and shaken at 4°C for 1 hour. Antibody should bind to C-myc of IL-10 binder candidate that should bind to IL-10 immobilized on microtitration plate.

After that, microtitration plates were 3x washed by wash buffer and into each well, 80 μl of TMB2-one step Turbo Solution was added. TMB2-one step solution is a peroxidase substrate which is metabolized by peroxidase built in mentioned antibody (see Figure 4).
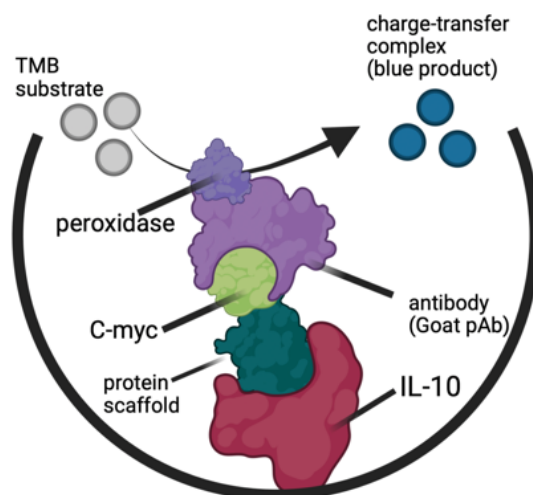
Figure 4: Schema of indirect ELISA principle used for ELISA screening (created by BioRender.com, 2023)

Reaction was stopped after 5 min by adding 40 µl of 2 M sulfuric acid into each well. Then, the absorbance at 450 nm was measured via Clario Star Microplate Reader. The values of absorbance are listed in appendix II. The degree of binding affinity between the scaffold and IL-10 should be directly proportional to the measure of absorbance.

4.2.3.8 Cultivation of best IL-10 binder candidates obtained from ELISA screening

According to previous ELISA screening, 12 best candidates (with highest absorbance) derived from F5_WT, recpectively G3_WT were inoculated from frozen glycerol microtitration plate stock into 2 ml of fresh LB medium with kanamycin and shaken at 180 x g 37 °C overnight. Then, plasmid DNA was isolated and purified via commercial kit (Plasmid Purification Plasmid Miniprep Kit I) and sequenced in the same way as described in section 4.2.3.2.4. The concentrations of plasmid DNA measured by spectrometer are listed in Table A6 in appendix III. Sequence analysis of these candidates was performed using the Biopython library (Cock *et al*. 2009) and MAFFT server (Katoh et al. 2002). The sequence alignment is listed in Figure A3, appendix II.

4.2.3.9 Sequence analysis via Biopython library

Amino acid sequences of F5 and G3 wildtypes were provided as text files. As result of clone sequencing, nucleotide sequences in .abi files were obtained. Using namely Biopython (Cock *et al*. 2009) library, nucleotide sequences were translated into amino acid sequences. For both F5 and G3 candidates, fasta files containing amino acid sequences for wildtype and corresponding clones were created (see Figure A3 in appendix II and appendix IV).

Fasta file for each candidate was loaded to MAFFT server (Katoh *et al*. 2002) for multiple sequence alignment, where wildtype was selected as alignment consensus sequence. Results were obtained in .fasta fomat.

4.2.3.10 Purification of IL-10 binding variants selected via ELISA screening

Three best IL-10 binder candidates F5_A2, F5_F7, F5_E9, G3_D4, G3_B11 and G3_E9 were chosen according to their sequence and estimated binding properties. Then, transformation of plasmid DNA encoding these chosen candidates and also F5_WT and G3_WT into chemically competent cells BL23GOLD was performed in the same way as described in Section 4.2.2.1.

From fresh agar plates with kanamycin and grown cell colonies, the cells were inoculated into 2.5 ml of fresh LB medium with kanamycin and allowed to grow overnight in heated shaking thermobox at 180 x g, 37°C. Next morning, 2 ml of culture was inoculated into 200 ml of kanamycin LB medium, shaken at 37°C and 120 x g until the OD value reached 0.55. the temperature of the shaking incubator was decreased to 18 °C, the cell culture was induced by IPTG (final concentration was 1 mM) 1 for protein production and shaken at 120 x g overnight.

Next morning, cells were transferred into a 50 ml tube and centrifuged at 5000 x g for 15 min; the supernatant was then discarded. The cells were washed with 15 ml of buffer (50 mM Tris, pH 8.0; 300 mM NaCl) and centrifuged again at 5000 x g. After decanting the supernatant, the cells were resuspended in buffer (50 mM Tris, pH 8.0; 300 mM NaCl) and sonicated using a Q-Sonica sonicator to break open cell membranes. The amplitude of the sonicator instrument was set to 5, pulse on time was 2 seconds, pulse off time was 4 seconds, and process time 7 min.

After sonication, cells with broken cell membranes in solution were centrifuged at 40000 x g, 4 °C for 18 min. In the next step, a column containing Streptactin XT matrix was equilibrated using column equilibration buffer (50 mM Tris, pH 8.0; 150 mM NaCl; 1 mM EDTA). Then, the centrifuged supernatant was loaded into the column resin. The column containing the loaded supernatant was washed by the same equilibration buffer. Then proteins were eluted by 3 ml of BXT buffer into 5 ml sterile plastic tubes.

The purity of chosen candidates was verified through SDS-PAGE in the same way as listed in section 4.2.1.7.

4.2.3.11 ELISA binding assay

ELISA binding assay was performed as described in the section 4.2.3.7, appart from purified IL-10 binding variants (see previous pharagraph) were used instead of cell lysate, and concentration of those IL-10 binding variants was 150 µg/ml. The gained values of absorbance are listed in Table 20. F5_A2 variant was selected for size exclusion chromatography and more accurate binding affinity measurement by microscale thermophoresis (MST).

4.2.3.12 Size exclusion chromatography purification of F5_A2 clone

Protein sample eluted in BXT elution solution was concentrated in the same way as described in section 4.2.1.5.

Size exclusion chromatography purification was performed as described in section 4.2.1.6. The purity verification of fractions 17-19 (depicted in Figure 12) by SDS-PAGE was performed in the same way as described in paragraph 4.2.1.7.

4.2.4   Affinity measurement of A2_F5 to IL-10 via microscale thermophoresis

First, 8 ml of dH$_2$O was added into vial containing 2 ml of 5x concentrated PBS-T (Monolith protein labeling kit red-tris-Nta). Then, fluorescent dye (Monolith protein labeling kit red-tris-Nta) was suspended in 50 µl of PBS-T to obtain 5µM dye solution. In the next step, 5 µM dye solution was diluted in 98 µl of PBS-T to obtain 100 mM dye solution.

IL-10 (3076 µg/ml) in volume of 0.110 µl was diluted in 99.9 µl of 1% Pluronic 50 mM Tris 300 mM NaCl solution. Therefore, final concentration of IL-10 was 200 nM. 100 µl of 200 mM Il-10 was mixed with 100 mM dye solution, put into dark and incubated for 30 min at room temperature. Centrifuge was pre-cooled at 4°C. After that, Il-10 sample was spined at 15,000 x g for 10 min.

In the next step, 16 PCR microtubes were prepared. Into the first one, 25 µl of 26.6 µM ligand (F5_A2) was pipetted; 10 µl of this was then transferred to the second tube, and 10 µl of 1 % Pulronic 50 mM Tris 300 mM NaCl solution and 26.6 µM ligand from the first tube were added to obtain 13.3 µM in the third tube. For each subsequent tube, 10 µl of ligand from the previous one and 10 µl of 1 % Pluronic 50 mM Tris 300 mM NaCl solution were pipetted for a 2x dilution in every step. Then, into each tube, 10 µl of labeled IL-10 sample was added. Finally, capillaries were filled with these solutions and placed into an instrument; LED power was set at 40 %, MST power was set at 20 %.

4.2.5   Hydrophobicity calculation of selected and screened F5 and G3 clones via Biopython library

Fasta files containing alignments were analyzed by Biopython library (Cock *et al*. 2009). For F5_WT and G3_WT and their corresponding variants diversified by error-prone PCR and selected through ribosome display and ELISA screening selection methods, hydrophobicity of positions of theoretical alpha helix formation was calculated. Positions of theoretical alpha helix formation were determined by available 3D Protein Feature View obtained from wwPDB.org (Berman *et al*. 2000) of 4PSF protein, which is parental protein of 57aBi protein scaffold (from which F5_WT and G3_WT proteins were derived). Mean value of hydrophobicity parameter of the variants was compared to value of the wildtype. Comparison was conducted by two-sided

non parametric t-test method. Null hypothesis stating equality of mean value and wildtype value was tested on confidence level 95 % (see appendix V).

5 Results

5.1 IL-10 purification

Affinity chromatography run through His-trapTM column is shown in Figure 5. Fractions 34-43 (see Figure 5) were purified via size exclusion chromatography by Superdex column. Run of size exclusion chromatograpy of concentrated fractions 34-43 is depicted in Figure 6. Concentrations of obtained size exclusion chromatography purified fractions of IL-10 18, 19 and 20 are listed in Table 18. Purity of fractions 13-15 and 18-20 were determined via SDS-PAGE (see picture of SDS-PAGE gel in Figure 7). Figure 7 shows that protein samples from fractions 13-15 contained impurities, fractions 18-20 contain impurities to a lesser excent. In Figure 7 can be also seen fractions of dimer form of IL-10 corresponding to an apparent molecular weight 37 kDa.
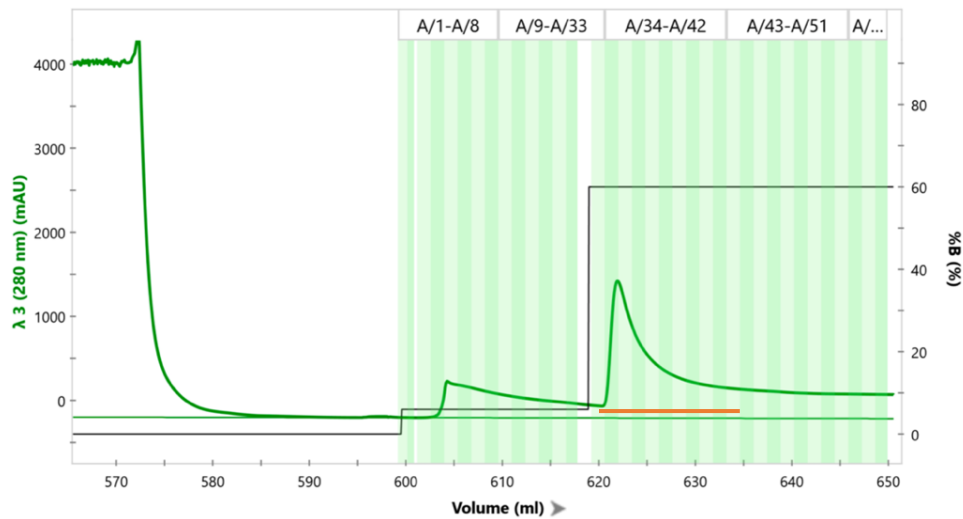

Figure 5: Affinity chromatography run for IL-10 protein. Orange line highlights fractions 34-43 which were concentrated and purified via size exclusion chromatography.
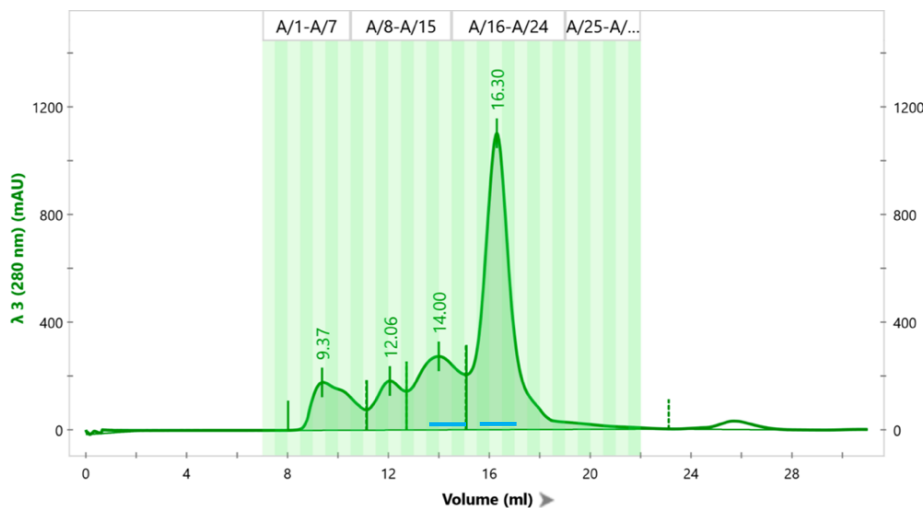

Figure 6: Size exclusion chromatography run for IL-10. Blue lines highlight fractions 13-15 and 18-20, which were analyzed via SDS-PAGE.
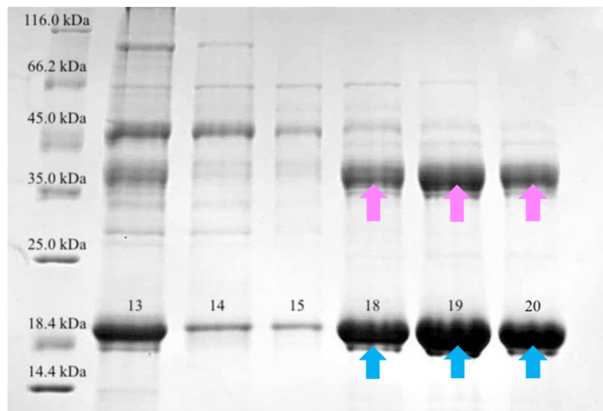
Table 18: Concentrations of purified fractions of IL-10

Fraction n.	c [mg/ml]
18	2.32
19	4.00
20	3.41

Figure 7: SDS-PAGE of purified fractions of IL-10 13-14 and 18-20. Theoretical molecular weight of IL-10 is 19 955 Da. Pink arrows highlight dimer form of IL-10 in fractions 18-20 corresponding to apparent molecular weight 37 kDa, blue arrows highlight monomeric form of IL-10 corresponding to apparent molecular weight 19kDa.

5.2   Library diversification by Error-prone, sequence analysis

Via sequence analysis, using SnapGene program and online converter ExPASy (Gasteiger *et al*. 2003), it was found that 75 % alignments of sequenced constructs pRDVsm_F5_EP contained nonsynonymous mutations and the average number of mutations was 1.75 amino acids per DNA construct exchanged.

Sequenced constructs pRDVsm_G3_EP contained 71 % of nonsynonymous mutations and the average number of mutations was 1.28 amino acids changes per DNA construct. Sequence alignment is listed in Figure A, appendix II.

5.3   Ribosome display selection

Through ribosome display were successfully selected IL-10 binding clones derived from F5_WT and G3_WT diversified by error-prone PCR. Verification that the entire ribosomal display method had been performed correctly and 406 bp long variants F5_sel and G3_sel were generated after final PCR was performed through agarose gel electrophoresis (see Figure 8).

Figure 8: Agarose electrophoresis of F5_sel and G3_sel fragments.

51

5.4 ELISA screening

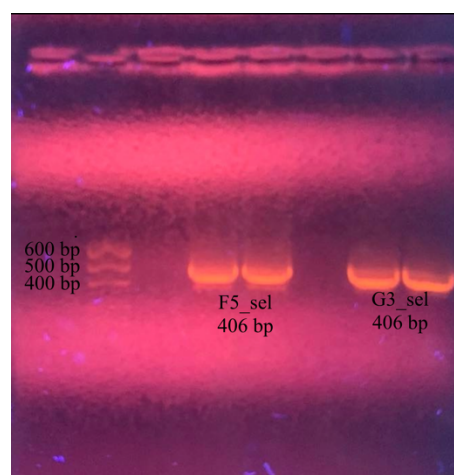By measurement of absorbance with ClarioStar instrument of the yellow-colored products of the ELISA screening assay at 450 nm, it was found that 60 % of clones derived from F5_WT showed higher absorbance than F5_WT, and 45% of clones derived from G3_WT showed higher absorbance than G3_WT. Absorbance values assigned to individual clones are listed in Figure A1, appendix I. From this screening, 12 best candidates with greatest absorbance derived from F5_WT, respectively from G3_WT were chosen for sequence analysis.

5.5 Sequence analysis of ELISA screened clones via Biopython library

Via sequence analysis performed with using Biopython library (Cock *et al*. 2009) it was found that clones obtained by ribosome display and ELISA screening selection, contained significantly higher amount of amino acid changes.

These mutations were distributed exactly on sections of mutable amino acid residues (see Figure 9 and Figure A3 in appendix II) that comes from parental 57aBi protein scaffold wild type design.

F5_WT	R	L	V	I	T	I	A	L	R	G	L	E	L	K	Y	P	L	C	L	R	P	A	W	H
F5_A2	M	L	V	I	F	I	A	C	H	G	L	E	H	K	Y	R	L	I	L	F	P	Y	W	S
F5_A12	A	L	V	I	R	I	A	G	A	G	L	E	A	K	Y	A	L	F	L	T	P	S	W	E
F5_E9	L	L	V	I	V	I	A	C	H	G	L	E	R	K	Y	C	L	P	L	K	P	T	W	V
F5_F1	D	L	V	I	S	I	A	R	A	G	L	E	F	K	Y	V	L	V	L	R	P	Q	W	F
F5_F7	G	L	V	I	S	I	A	G	R	G	L	E	R	K	Y	W	L	V	L	A	P	P	W	I
F5_H5	G	L	V	I	S	I	A	G	R	G	L	E	R	K	Y	W	L	V	L	A	P	P	W	I
F5_H6	P	L	V	I	Q	I	A	T	F	G	L	E	R	K	Y	Y	L	H	L	G	P	K	W	L

	96	97	98	99	100	101	102	103	104	105	106	107	108	109	110	111	112	113	114	115	116	117	118	119
G3_WT	R	L	V	I	A	I	A	P	N	G	L	E	R	K	Y	T	L	H	L	T	P	T	W	S
G3_A3	Y	L	V	I	L	I	A	A	Q	G	L	E	L	K	Y	F	L	A	L	L	P	N	W	P
G3_A4	L	L	V	I	R	I	A	L	P	G	L	E	G	K	Y	N	L	S	L	M	P	D	W	P
G3_C2	K	L	V	I	N	I	A	Y	Q	G	L	E	G	K	Y	S	L	L	L	F	P	S	W	I
G3_D4	T	L	V	I	Y	I	A	L	C	G	L	E	C	K	Y	V	L	I	L	H	P	G	W	H
G3_E5	S	L	V	I	N	I	A	V	E	G	L	E	W	K	Y	V	L	S	L	S	P	L	W	L
G3_E9	P	L	V	I	A	I	A	F	S	G	L	E	T	K	Y	T	L	R	L	N	P	T	W	F
G3_G4	L	L	V	I	G	I	A	A	S	G	L	E	G	K	Y	S	L	L	L	R	P	H	W	L
G3_H10	L	L	V	I	F	I	A	T	R	G	L	E	S	K	Y	G	L	Q	L	C	P	V	W	L

Figure 9: Alignment of G3_WT (blue highlighted) and F5_WT (green highlighted) derived variants via error-prone PCR diversification and ribosome display, ELISA screening selection. Sections of mutated amino acids are highlighted in light blue. Positions 96-110 should be corresponding to theoretical alpha helix formation of secondary structure of G3_WT and F5_WT variants. Based on www.rscb.org (Berman et al. 2000).

5.6 Affinity chromatography of best ELISA screened IL-10 binder candidates

Variants F5_A2, F5_F7, F5_E9, G3_E9, G3_D4 and G3_B11 that showed the highest absorbance value measured with ClarioStar instrument from ELISA screening were produced in BL23GOLD cells and purified through Streptactin XT matrix column. F5_WT and G3_WT were purified too. Purity of variants was verified by SDS-PAGE. Picture of SDS-PAGE gel is depicted in Figure 10, where can be seen that obtained protein samples contained some

impurities after purification. Chosen purified IL-10 binder variants and their determined concentrations are listed in Table 19.
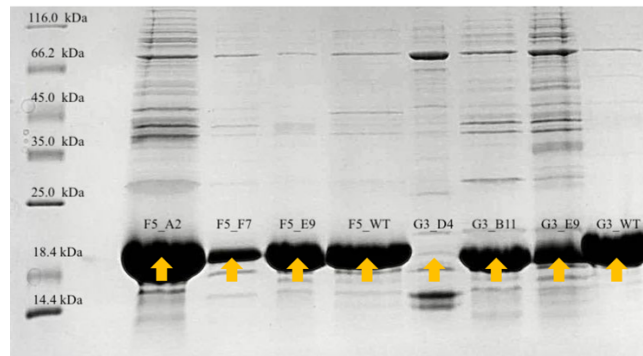

Figure 10: SDS-PAGE of chosen ELISA screened protein IL-10 binder candidates. Yellow arrows highlight fractions of IL-10 binder candidates. Theoretical molecular weights of IL-10 binder candidates: F5_A2: 17.3 kDa; F5_F7: 17.1 kDa; F5_E9: 17.1 kDa; F5_WT: 17.2 kDa; G3_B11: 16.9 kDa; G3_D4: 17.1 kDa; G3_E9: 17.1 kDa; F3_WT: 17.1 kDa. Apparent molecular weight of highlighted fractions is approximately 19 kDa.

Table 19: concentrations of purified chosen
IL-10 binder candidates and their wild types

Protein	c [mg/ml]
F5_A2	3.20
F5_F7	0.43
F5_E9	1.23
F5_WT	1.27
G3_B11	0.64
G3_D4	1.39
G3_E9	1.77
G3_WT	2.12

5.7 ELISA binding assay

Measured values of absorbance at 450 nm of yellow-colored products of ELISA binding assay showed, that variants A2_F5, G4_D4 and G3_E9 showed significantly higher absorbance than their wild types at the 80 % confidence level. This result was obtained by one-sided nonparametric t-test. Null hypothesis was stated as equality of wild type absorbance and mean absorbance of the clones. Samples were analyzed in triplicates. Average values of absorbance of each measured triplicate sample are shown in Figure 11, statistical summary of absorbance values are listed in Table 20.
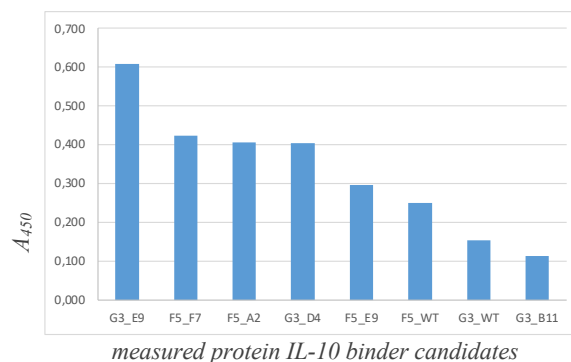

measured protein IL-10 binder candidates

Figure 11: Average absorbances of values of chosen IL-10 binder candidates at 450 nm.

Table 20: Statistical summary of absorbance values obtained via ELISA binding assay.

Name of IL-10 binder candidate	Median	80% Confidence level
F5_F7	0.423	(0.309, 0.537)
F5_A2	0.406	(**0.340**, 0.473)
F5_E9	0.296	(0.255, 0.338)
F5_WT	0.250	(0.182, **0.318**)
G3_B11	0.112	(0.102, 0.122)
G3_D4	0.404	(**0.298**, 0.510)
G3_E9	0.607	(**0.450**, 0.765)
G3_WT	0.153	(0.139, **0.167**)

5.8 Size exclusion chromatography of F5_A2 protein scaffold candidate

From ELISA binding assay, F5_A2 protein IL-10 binder candidate was chosen for purification via size exclusion chromatography by Superdex column. The chromatography run in the Figure 12 shows that fractions 17-19 were enriched by the eluted F5_A2 binder. According to column characterization, fractions 1-16 contained possible aggregates or impurities with a larger molecular weight than that of the F5_A2 binder. Purity of fractions 17-19 was verified by SDS-PAGE . Concentration of fractions 17-19 are listed in Table 21.
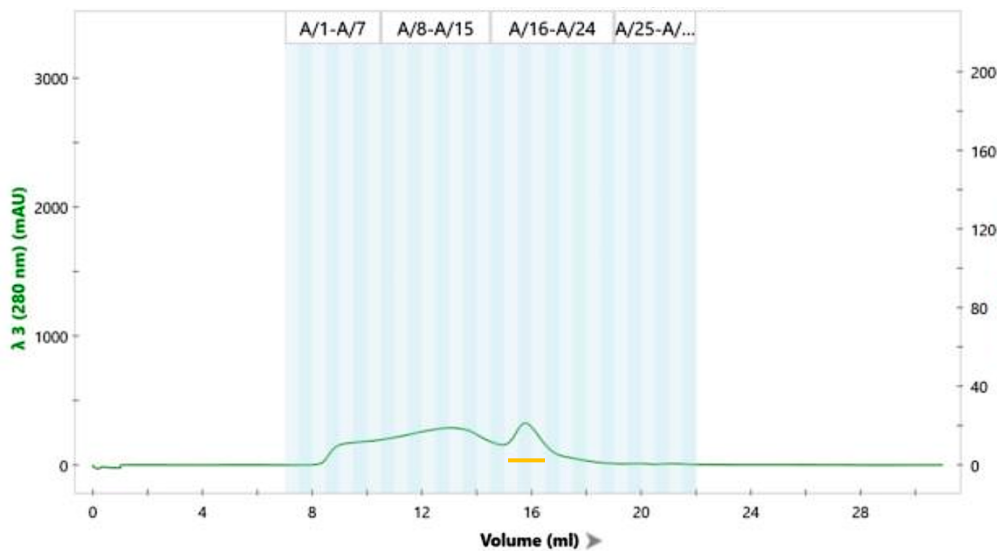

Figure 12: Size exclusion chromatography run of F5_A2 protein scaffold. Yellow line highlights fractions 17-19 which were analyzed through SDS-PAGE.

Purity of fractions 17, 18 and 19 was determined through SDS-PAGE (see Figure 13). As it can be seen in Figure 13, the fraction 19 contained minimum impurities.
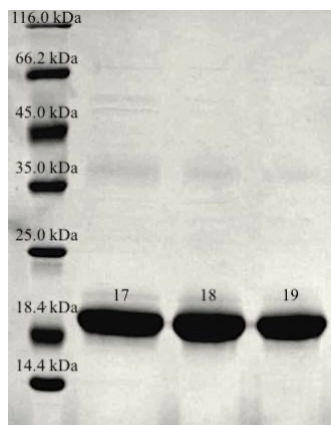
Table 21: Concentrations of fractions 17-19 of purified F5_A2 protein binder.

Fraction n.	c [mg/ml]
17	0.49
18	0.57
19	0.46

Figure 13: SDS-PAGE of fractions 17-19 riched by the F5_A2 protein binder purified via affinity chromatography and size exclusion chromatography. The theoretical molecular weight of F5_A2 is 17.3 kDa, apparent molecular weight of fractions 17-19 is approximately 19 kDa.

5.9 Binding affinity of F5_A2 protein IL-10 binder candidate to IL-10 via MST

Binding affinity of F5_A2 binder to IL-10 was determined through dissociation constant K_d:

$$K_d = \frac{[IL10] \cdot [F5\_A2]}{[IL10F5\_A2]}$$

Binding curve of F5_A2 binder to IL-10 expressing the change of fluorescence with increasing F5_A2 binder concentration is shown in Figure 14. Fluorescence increases with increasing binder concentration. Measured dissociation constant K_d of F5_A2 binder determined from binding curve is 730 ± 60 nM.
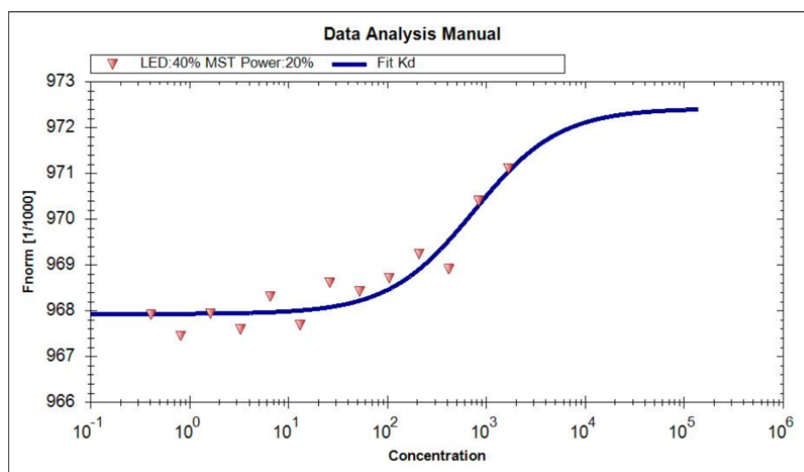
Figure 14: Binding curve of F5_A2 to IL-10 expressing the increase of fluorescence with increasing F5_A2 ligand concentration, x-axis presents F5_A2 concentration [nM], y-axis presents change of fluorescence.

5.10 Hydrophobicity calculation through Biopython library

Using Biopython library (Cock *et al.* 2009) it was found that variants derived from G3_WT obtained by error-prone PCR diversification and also by ribosome display and ELISA screening selection methods provide on 95% confidence level significantly higher hydrophobicity than

hydrophobicity of G3_WT in theoretical area of alpha helix, as it can be seen in Table 22 and 23. Hydrophobicity of clones sequenced before selection methods performance was not significantly higher than G3_WT. Hydrophobicity of clones obtained from F5_WT was not significantly increased neither after error-prone PCR nor selection methods performance (see Table 22 and 23). Alignment of G3_WT derived clones via error-prone PCR, selected by ribosome display and ELISA screening is depicted in Figure 9. In Figure 15, the light green highlighted mutated amino acid positions in alpha helix area of G3_WT construct can be seen.

Table 22: Calculated hydrophobicity for sequences of variants derived from wildtypes F5_WT, G3_WT

Names of sequences derived from F5_WT, G3_WT	Median of theoretical alpha helix hydrophobicity	95% Confidence level
F5EP	0.493	(0.417, 0.569)
G3EP	0.049	(-0.022, 0.121)
F5RE	0.450	(0.187, 0.713)
G3RE	0.633	**(0.372, 0.914)**

F5EP: Sequences of variants derived from F5_ WT via error-prone PCR diversification; G3EP: Sequences of variants derived from G3_WT via error-prone PCR diversification; F5RE: Sequences of variants derived from F5_WT by error-prone PCR diversification, ribosome display and ELISA screening selection; G3RE: Sequences of variants derived from G3_WT by error-prone PCR diversification, ribosome display and ELISA screening selection.

Table 23: Calculated hydrophobicity of F5_WT and G3_WT wildtypes.

Name of sequence	Alpha helix hydrophobicity
F5_WT	0.526
G3_WT	-0.011

Figure 15: Light green highlighted mutated amino acids positions in helix area of G3_WT construct diversified by error-prone PCR, selected via ribosome display and ELISA screening selection methods. Obtained from wwPDB.org (Berman et al. 2000).

6 Discussion

Via directed evolution methods, second generation of protein IL-10 binder candidates binding IL-10 was developed. Protein scaffolds F5_WT and G3_WT, derived from parental 57aBi protein scaffold (Pham *et al*. 2021) developed in Laboratory of biomolecular recognition, were used as templates to generate diversified DNA libraries. From these libraries variants with IL-10 binding capabilities were selected using ribosome display and ELISA screening selection methods.

Recombinant human IL-10 containing His-tag in its structure, produced by successfully transfected Schneider 2 cell line, was purified by affinity and size exclusion chromatography. Purity of obtained resulted fractions 18, 19 and 20 was verified by SDS-PAGE (see Figure 7). In the Figure 7, monomeric and dimeric forms of IL-10 can be seen. Fraction number 20 was selected for further measurements, all fractions were frozen by liquid nitrogen and stored at -80°C.

For libraries derived from F5_WT and G3_WT diversification, error-prone PCR solution was optimized so that 1-4 amino acid changes per sequence were produced. This is in accordance with the recommended number of changed amino acids for improving protein properties through directed evolution (Wong *et al*. 2006). Desired amount of amino acid changes performed by error-prone PCR was proved by sequence analysis via Snapgene program and ExPASy online translate tool (Gasteiger *et al*. 2003). As it can be seen in Figure A2 in appendix II, nonsynonymous mutations were randomly distributed. Moreover, based on sequence analysis by Biopython library (Cock *et al*. 2009), hydrophobicity of obtained diversified libraries did not significantly change (see Table 22 and 23), which is also described in the available literature (Ruff *et al*. 2014).

On the other hand, Biopython library (Cock *et al*. 2009) using sequence analysis of diversified libraries subjected to ribosome display selection and ELISA screening showed that mutations are highly concentrated in certain positions (see Figure 9). The mutation sites correspond to the positions of mutable amino acid residues of the parental 57aBi wildtype scaffold, from which F5_WT and G3_WT were derived (Pham *et al*. 2021). Also, it was found that the average number of nonsynonymous mutations of obtained resulted variants was distinctly increased to value of 10 amino acid changes per sequence (see Figure A2 and A3 in appendix II).

It is interesting, that by Biopython library (Cock *et al*. 2009) calculation, resulted clones derived from G3_WT by error-prone PCR diversification, ribosome display and ELISA screening selection methods showed significantly higher hydrophobicity in alpha helix section

than G3_WT itself (see Table 22, Table 23 and Figure 15) at 95 % confidence level. Hydrophobic core sections that ensure protein stability (Dijk *et al*. 2015) appear mainly in alpha helices of proteins (Lu *et al*. 2011). This fact may suggest that the resulting clones derived from G3_WT obtained via directed evolution process could gain higher stability.

Based on the findings about a showed increase of the frequency of amino acids changes appearing in variants after ribosomal display and ELISA screening selection, it can be confirmed that selection methods are an important element of directed evolution methods. Utilization of ribosomal display method is, among other things, effective tool for selection of functional variants of clones that have not undergone changes incompatible with the production of the protein they encode due to previous random mutagenesis diversification.

The result of the ELISA screening suggests that 60% of the newly developed resultant variants derived from F5_WT and 45% resultant clones derived from G3_WT could provide a greater affinity to IL-10 than their parental wildtype molecules based on higher absorbance assigned to corresponding clone within ELISA screening (see Figure A1, appendix I). From ELISA screening, twelve best clones were selected based on their absorbance level and the quality of their sequencing. As mentioned before, based on sequence alignment, it was possible to observe increased numbers of changed amino acids at certain positions corresponding to mutable patches of 57aBi wildtype.

Chosen clones F5_A2, F5_F7, F5_E9, G3_E9, G3_D4 and G3_B11 were purified via affinity chromatography by streptactin XT binding strep-tag, which was incorporated in constructs of chosen variants. Purity of chosen variants was verified through SDS-PAGE (see Figure 10). All variants except F5_D4 variant were purified. F5_D4 variant could not be purified using standard method. However, the streptactin XT column purification process did not eliminate impurities from the resulting samples. Impurities may have been present in the sample due to imperfect purification through the streptactin XT matrix on the column. Purified variants were used for ELISA binding assay.

The result of ELISA binding assay showed that although the average values (see Figure 11) provided greater absorbance (and possible affinity to IL-10), only clones F5_A2, G3_D4 and G3_E9 showed significantly higher absorbance and therefore affinity at the 80 % confidence level (see Table 20). The resulting large deviations in the measured absorbance of triplicate samples were influenced by a technical problem with automatic microtitration plate washer and subsequent possible human error during manual washing of plate during ELISA binding assay, which may have contributed to the error.

To determine more accurate binding affinity of binder(s) to IL-10 we decided to use MST measurement of the affinity and size exclusion chromatography purified F5_A2 variant. Purity

of obtained fractions 17, 18 and 19 of purified F5_A2 binder candidate was verified by SDS-PAGE (see Figure 13). In Figure 13, it can be seen that protein F5_A2 purified by affinity chromatography and size exclusion chromatography showed higher purity than the same protein purified just by the affinity chromatography (purity of F5_A2 protein purified only by affinity chromatography is depicted in Figure 10).

Because of His-tag carried by IL-10, which can be fluorescently tagged, the thermophoresis of IL-10 bound to F5_A2 could be detected (see binding curve depicted in Figure 14). Dissociation constant of F5_A2 binder was determined to be 730 ± 56 nM which is more than 100x higher value than the dissociation constant value of parental IL-10 binder F5_WT determined to be 6 nM (Pham *et al*. 2021). This indicates that the affinity of F5_A2 to IL-10 is significantly weaker than binding affinity of F5_WT to IL-10. Unfortunately, this result is negatively influenced by a long storage time of IL-10 under adverse conditions at 4 °C. Fraction n. 20 of purified IL-10 intended for MST binding affinity measurement was also intended for ELISA screening and ELISA binding assay, whereas two months passed from the purification of IL-10 to the MST measurement, and the laboratory could not schedule the MST measurement earlier. Subsequently, we realized that IL-10 degrades over the course of a month when stored at 4 °C (www.rndsystems.com, 2023, online). To obtain an accurate assessment of the binding affinity of F5_A2 to IL-10, MST measurement should be repeated using freshly purified IL-10 and F5_A2 proteins. Nevertheless, the error-prone PCR library diversification, ribosomal display and ELISA screening selection techniques were successfully performed for second-generation IL-10 binder obtainment.

By obtaining a binder with a greater affinity for IL-10, further opportunities for its potential use in the diagnosis or treatment of various civilization diseases such as atherosclerosis, different types of cancer, rheumatoid arthritis, and others (Liu *et al*. 2021) can be provided. Due to their smaller size, protein scaffolds are better at permeating biological membranes compared to traditional antibodies. They can also provide great stability or binding affinity to target molecules (Luo *et al*. 2022). Additionally, replacing traditional antibodies with protein scaffolds in therapy could mean better access to drugs for more patients. Last but not least, producing protein scaffolds is more environmentally friendly than traditional antibody production, because of *E. coli* protein scaffold production possibility.

7 Conclusion

The goal of this thesis was development of second-generation proteins binding human IL-10, clinically important cytokine whose altered levels in the body reflect various civilization diseases and tumor cells.

Newly developed binders to IL-10 were based on 57aBi scaffolds developed in the laboratory (Pham *et al*. 2021). They were derived from the F5 and G3 variants of the parental 57aBi wild type scaffold protein via directed evolution methods. The affinity of the resulting variants to IL-10 was measured by microscale thermophoresis, MST.

In this work, I show that via directed evolution selection methods including ribosome display and ELISA screening, clones with a significantly increased number of changed amino acids at certain positions were selected from diversified library containing prevailing 1-4 amino acid changed variants. Also, the binding affinity of chosen clone F5_A2 to IL-10 was measured through MST measurement. Although the measured affinity of resulting protein scaffold F5_A2 did not confirm significant improvement of binding compared to the original variant F5_WT, repetition of the MST measurement with freshly purified proteins could yield a better binding affinity values.

8 Literature

Aguinaldo AM, Arnold FH. 2003. Staggered extension process (StEP) in vitro recombination. Methods in Molecular Biology **192**:235-239.

Arnoux B, Ducruix A, Prange T. 2002. Anisotropic behaviour of the C-terminal Kunitz-type domain of the alpha3 chain of human type VI collagen at atomic resolution (0.9 A). Acta Crystallographica Section D **58**:1252-1254.

Ahmadi MKB, Mohammadi SA, Makvandi M, Mamouei M, Rahmati M, Dehghani H, Wood DW. 2021. Recent Advances in the Scaffold Engineering of Protein Binders. Current Pharmaceutical Biotechnology **22**:878-891.

Bagchi AK, Surendran A, Malik A, Jassal DS, Ravandi A, Singal PK. 2020. IL-10 attenuates OxPCs-mediated lipid metabolic responses in ischemia reperfusion injury. Nature scientific report (32694752) DOI: 10.1038/s41598-020-68995-z.

Bachman J. 2013. Site-directed mutagenesis. Methods in Enzymology **529**:241-248.

Barkovskiy M, Ilyukhina E, Dauner M, Eichinger A, Skerra A. 2019. An engineered lipocalin that tightly complexes the plant poison colchicine for use as antidote and in bioanalytical applications. Biological Chemistry **400**:351-366.

Berman HM, J. Westbrook J, Feng Z, Gilliland G, Bhat TN, Weissig H, Shindyalov IN, Bourne PE. 2000. The Protein Data Bank. Nucleic Acids Research **28**: 235-242.

Boder ET, Wittrup KD. 1997. Yeast surface display for screening combinatorial polypeptide libraries. Nature Biotechnology **15**:553-557.

Brilland B, Bach-Bunner M, Gomes CN, Larochette V, Foucher E, Plaisance M, Saulnier P, Costedoat-Chalumeau N, Ghillani P, Belizna C, Delneste Y, Augusto JF, Jeannin P. 2021. Serum Interleukin-26 Is a New Biomarker for Disease Activity Assessment in Systemic Lupus Erythematosus. Frontiers in Immunology (34054830) DOI: 10.3389/fimmu.2021.663192.

Cao L, Wang W, Jiang Q, Wang C, Knossow M, Gigant B. 2014. The structure of apo-kinesin bound to tubulin links the nucleotide cycle to movement. Nature Communications (25395082) DOI: 10.1038/ncomms6364.

Castro F, Cardoso AP, Gonçalves RM, Serre K, Oliveira MJ. 2018. Interferon-Gamma at the Crossroads of Tumor Immune Surveillance or Evasion. Frontiers in Immunology **9**:1664-3224.

Chen W, Xing J, Liu X, Wang S, Xing D. 2021. The role and transformative potential of IL-19 in atherosclerosis. Cytokine & Growth Factor Reviews **62**:70-82.

Cock PJ, Antao T, Chang JT, Chapman BA, Cox CJ, Dalke A, Friedberg I, Hamelryck T, Kauff F, Wilczynski B, de Hoon MJ. 2009. Biopython: freely available Python tools for computational molecular biology and bioinformatics. Bioinformatics **25**:1422-1423.

Cotten SW, Zou J, Wang R, Huang BC, Liu R. mRNA display-based selections using synthetic peptide and natural protein libraries. Methods in Molecular Biology **805**:287-297.

Creative Biolabs. 2022. Protein Engineering Services: Cell Surface Display Systems for Protein Engineering. Available from https://www.creative-biolabs.com/Cell-Surface-DisplaySystems-for-Protein-Engineering.html (accessed May 2022).

Direct evolution. 2019. Protein Expression: Methods for tirected evolution of proteins. Sigma-Aldrich. Available from https://www.sigmaaldrich.com/NO/en/technical-documents/technical-article/protein-biology/protein-expression/directed-evolution (accessed November 2022).

Dudakov JA, Hanash AM, van den Brink MR. 2015. Interleukin-22: immunobiology and pathology. Annual Review of Immunology **33**:747-785.

Ebersbach H, Fiedler E, Scheuermann T, Fiedler M, Stubbs MT, Reimann C, Proetzel G, Rudolph R, Fiedler U. 2007. Affilin-novel binding molecules based on human gamma-B-crystallin, an all beta-sheet protein. Journal of Molecular Biology **372**:172-185.

Ebrahimizadeh W, Rajabibazl M. 2014. Bacteriophage vehicles for phage display: biology, mechanism, and application. Current Microbiolgy **69**:109-120.

Edelheit O, Hanukoglu A, Hanukoglu I. 2009. Simple and efficient site-directed mutagenesis using two single-primer reactions in parallel to generate mutants for protein structure-function studies. BMC Biotechnology (19566935) DOI: 10.1186/1472-6750-9-61.

Eigenbrot C, Ultsch M, Dubnovitsky A, Abrahmsen L, Hard T. 2010. Structural basis for high-affinity HER2 receptor binding by an engineered protein. Proceedings of the National Academy of Sciences of the United States of America **107**:15039-15044.

Fass D, Blacklow S, Kim PS, Berger JM. 1997. Molecular basis of familial hypercholesterolaemia from structure of LDL receptor module. Nature **388**:691-693.

Fernandez EJ, Lolis E. 2002. Structure, function, and inhibition of chemokines. Annual Review of Pharmacology and Toxicology **42**:469-499.

Fernandez PR, Kaski JC. 2002. Interleukin-10 and coronary disease. Revista Espanola de Cardiologia **55**:738-750.

Ferreira LV, Borba HHL, Bonetti FA, Leticia P, Pontarolo L, Pontarolo P. 2019. Cytokines and Interferons: Types and Functions. Chapter 4 in Ali Khan W, editor. Autoantibodies and Cytokines, IntechOpen, Saudi Arabia.

Fiorentino DF, Bond MW, Mosmann TR. 1989. Two types of mouse T helper cell. IV. Th2 clones secrete a factor that inhibits cytokine production by Th1 clones. Journal of Experimental Medicine **170**:2081-2095.

Gajdacs M, García-Perdomo AH, Sarshar M. (2021). 67-87 in Behzadi editor. A World of Wonders: Interleukin-1 (IL-1) and IL-2 Families. Interleukins – The Immune and Non-Immune Systems' Related Cytokines. IntechOpen, Saudi Arabia.

Gasteiger E, Gattiker A, Hoogland C, Ivanyi I, Appel RD, Bairoch A. 2003. ExPASy: The proteomics server for in-depth protein knowledge and analysis. Nucleic Acids Research **31**:3784-3788.

Gebauer M, Schiefner A, Matschiner G, Skerra A. 2013. Combinatorial design of an Anticalin directed against the extra-domain b for the specific targeting of oncofetal fibronectin. Journal of Molecular Biology **425**:780-802.

Gebauer M, Skerra A. 2020. Engineered Protein Scaffolds as Next-Generation Therapeutics. The Annual Review of Pharmacology and Toxicology **60**:391-415.

Gery I, Waksman BH. 1972. Potentiation of the T-lymphocyte response to mitogens. II. The cellular source of potentiating mediator(s). Journal of Experimental Medicine **136**:143-55.

Goldberg SD, Cardoso RM, Lin T, Spinka-Doms T, Klein D, Jacobs SA, Dudkin V, Gilliland G, O'Neil KT. 2016. Engineering a targeted delivery platform using Centyrins. Protein Engineering Design & Selection **29**:563-572.

Gonzalez-Garza TM, Cruz-Vega ED, Maldonado-Bernal C. 2021. IL10 as Cancer Biomarker. Translational Research in Cancer (IntechOpen) DOI: 10.5772/intechopen.90806.

Gold JL, Walker J. 2013. Directed Evolution. Pages 325-327 in Maloy S, Hughes K, editors. DiBrenner's Encyclopedia of Genetics. Academic Press, San Diego.

Graber JJ, Dhib-Jalbut S. 2014. Interferons. Pages 718-723 in Aminoff JM, Daroff JB, editors. Encyclopedia of the Neurological Sciences. Academic press, San Diego.

Guler R, Svedmark SF, Abouzayed A, Orlova A, Löfblom J. 2020. Increasing thermal stability and improving biodistribution of VEGFR2-binding affibody molecules by a combination of in silico and directed evolution approaches. Scientific reports – Nature (33097752) DOI: 10.1038/s41598-020-74560-5.

Heitz A, Avrutina O, Le-Nguyen D, Diederichsen U, Hernandez JF, Gracy J, Kolmar H, Chiche L. 2008. Knottin cyclization: Impact on structure and dynamics. BMC Structural Biology (19077275) DOI: 10.1186/1472-6807-8-54.

Högbom M, Eklund M, Nygren PA. 2003. Nordlund P. Structural basis for recognition by an in vitro evolved affibody. Proceedings of the National Academy of Sciences of the United States of America **100**:3191-3196.

Horvath CM. 2004. The Jak-STAT pathway stimulated by interferon gamma. Science's signal transduction knowledge environment (15561980) DOI: 10.1126/stke.2602004tr8.

Hosse RJ, Rothe A, Power BE. 2006. A new generation of protein display scaffolds for molecular recognition. Protein Science **15**:14-27.

Hoyer W, Grönwall C, Jonsson A, Ståhl S, Härd T. 2008. Stabilization of a beta-hairpin in monomeric Alzheimer's amyloid-beta peptide inhibits amyloid formation. Proceedings of the National Academy of Sciences of the United States of America **105**:5099-5104.

Huliciak M, Biedermanova L, Berdar D, Herynek S, Kolarova L, Tomala J, Mikulecky P, Schneider B. 2023. Combined in vitro and cell-based selection display method producing specific binders against IL-9 receptor in high yields (36637991) DOI: 10.1111/febs.16726.

Hutchings AP, Diez D, Miranda-Saavedra D. 2013. The IL-10/STAT3-mediated anti-inflammatory response: recent developments and future challenges. Briefings in Functional Genomics **12**:489-498.

Jacobs SA, Diem MD, Luo J, Teplyakov A, Obmolova G, Malia T, Gilliland GL, O'Neil KT. 2012. Design of novel FN3 domains with high stability by a consensus sequence approach. Protein Engineering Design & Selection **25**:107-117.

Jang DI, Lee AH, Shin HY, Song HR, Park JH, Kang TB, Lee SR, Yang SH. 2021. The Role of Tumor Necrosis Factor Alpha (TNF-α) in Autoimmune Disease and Current TNF-α Inhibitors in Therapeutics. International Journal of Molecular Sciences **22**:2719-2724.

Jenko S, Dolenc I, Guncar G, Dobersek A, Podobnik M, Turk D. 2003. Crystal structure of Stefin A in complex with cathepsin H: N-terminal residues of inhibitors can adapt to the active sites of endo – and exopeptidases. Journal of Molecular Biology **326**:875-885.

Ji J, Day A. 2020. Construction of a highly error-prone DNA polymerase for developing organelle mutation systems. Nucleic Acids Research **48**:11868-11879.

Jiang J, Zhao M, Chang C, Wu H, Lu Q. Type I. 2020. Interferons in the Pathogenesis and Treatment of Autoimmune Diseases. Clinical Reviews in Allergy & Immunology **59**:248-272.

Joern JM. DNA shuffling. 2003. Methods in Molecular Biology **231**:85-89.

Jorgovanovic D, Song M, Wang L, Zhang Y. 2020. Roles of IFN-γ in tumor progression and regression: a review. Biomark Research (33005420) DOI: 10.1186/s40364-020-00228-x.

Jost C, Schilling J, Tamaskovic R, Schwill M, Honegger A, Plückthun A. 2013. Structural basis for eliciting a cytotoxic effect in HER2-overexpressing cancer cells via binding to the extracellular domain of HER2. Structure **21**:1979-1991.

Karatan E, Han Z, Kay B. 2005. Molecular Display Technologies. Pages 409-430 in Meyer RA editor. Encyclopedia of Molecular Cell Biology and Molecular Medicine. Wiley-VCH Verlag, Weinheim.

Kasakura S, Lowenstein L. A. 1965. Factor stimulating DNA synthesis derived from the medium of leukocyte cultures. Nature **208**:794-795.

Katoh K, Misawa K, Kuma K, Miyata T. 2002. MAFFT: a novel method for rapid multiple sequence alignment based on fast Fourier transform. Nucleic Acids Research **30**:3059-3066.

Keir M, Yi Y, Lu T, Ghilardi N. 2020. The role of IL-22 in intestinal health and disease. Journal of Experimental Medicine (32997932) DOI: 10.1084/jem.20192195.

Kohl A, Binz HK, Forrer P, Stumpp MT, Plückthun A, Grütter MG. 2003. Designed to be stable: crystal structure of a consensus ankyrin repeat protein. Proceedings of the National Academy of Sciences **100**:1700-1705.

Koide A, Abbatiello S, Rothgery L, Koide S. 2002. Probing protein conformational changes in living cells by using designer binding proteins: application to the estrogen receptor. Proceedings of the National Academy of Sciences of the United States of America **99**:1253-1258.

Koide A, Wojcik J, Gilbreth RN, Hoey RJ, Koide S. 2012. Teaching an old scaffold new trick: monobodies constructed using alternative surfaces of the FN3 scaffold. Journal of Molecular Biology **415**:393-405.

Kragstrup TW, Andersen T, Heftdal LD, Hvid M, Gerwien J, Sivakumar P, Taylor PC, Senolt L, Deleuran B. 2018. The IL-20 Cytokine Family in Rheumatoid Arthritis and Spondyloarthritis. Frontiers in Immunology (30319661) DOI: 10.3389/fimmu.2018.02226.

Labani-Motlagh A, Ashja-Mahdavi M, Loskog A. 2020. The Tumor Microenvironment: A Milieu Hindering and Obstructing Antitumor Immune Responses. Frontiers in Immunology (32499786) DOI: 10.3389/fimmu.2020.00940.

Lacy P. 2015. Editorial: secretion of cytokines and chemokines by innate immune cells. Frontiers in immunology (25954279) DOI: 10.3389/fimmu.2015.00190.

Lai Y, Dong C. 2016. Therapeutic antibodies that target inflammatory cytokines in autoimmune diseases. International immunology **28**:181-188.

Laursen K. 2016. Blog Addgene: Site Directed Mutagenesis by PCR. Cornell University. Available from https://blog.addgene.org/site-directed-mutagenesis-by-pcr (accessed January 2023).

Lee CG, Kim T, Hong S, Chu J, Kang JE, Park HG, Choi JY, Song K, Rha SY, Lee S, Choi JS, Kim SM, Jeong HM, Shin YK. 2021. Antibody-Based Targeting of Interferon-Beta-1 a Mutein in HER2-Positive Cancer Enhances Antitumor Effects Through Immune Responses and Direct Cell Killing. Frontiers in pharmacology (33505314) DOI: 10.3389/fphar.2020.608774.

Lee PA, Tullman-Ercek D, Georgiou G. 2006. The bacterial twin-arginine translocation pathway. The Annual Review of Microbiology **60**:373-395.

Lemmens LJM, Ottmann C, Brunsveld L. 2020. Conjugated Protein Domains as Engineered Scaffold Proteins. Bioconjugate Chemistry **31**:1596-1603.

Lindborg M, Dubnovitsky A, Olesen K, Bjorkman T, Abrahmsen L, Feldwisch J, Hard T. 2013. High-affinity binding to staphylococcal protein A by an engineered dimeric Affibody molecule. Protein Engineering Design and Selection **26**:635-644.

Liu C, Chu D, Kalantar-Zadeh K, George J, Young HA, Liu G. 2021. Cytokines: From Clinical Significance to Quantification. Advanced science (Weinheim) (34114369) DOI: 10.1002/advs.202004433.

Liu Y, Sorensen JB, Brun NC, Frejd FY, Tolmachev V. 2022. Theranostic pairing: ABY-025/251 targeting HER2 with 68Ga and 188Re—Minimized radioligands using Affibody peptide scaffold technology. Journal of Clinical Oncology **16**: 3093-3093.

Lorenz TC. 2012. Polymerase chain reaction: basic protocol plus troubleshooting and optimization strategies. The Journal of Visualized Experiments (22664923) DOI: 10.3791/3998.

Lu H, Wang J, Bai Y, Lang JW, Liu S, Lin Y, Cheng J. 2011. Ionic polypeptides with unusual helical stability. Nature (21343924) DOI: 10.1038/ncomms1209.

Luo R, Liu H, Cheng Z. 2022. Protein scaffolds: antibody alternatives for cancer diagnosis and therapy. RSC Chem Biol **3**:830-847.

Main AL, Harvey TS, Baron M, Boyd J, Campbell ID. 1992. The three-dimensional structure of the tenth type III module of fibronectin: an insight into RGD-mediated interactions. Cell press **71**:671-678.

Markota A, Endres S, Kobold S. 2018. Targeting interleukin-22 for cancer therapy. Human Vaccines & Immunotherapeutics **14**:2012-2015.

Mate DM, Gonzalez-Perez D, Mateljak I, Gomez de Santos P, Vicente AI, Alcalde M. 2017. Pages 185-213 in Brahmachari G, editor. Biotechnology of Microbial Enzymes. Academic press, USA.

Matsuura T, Yomo T. 2006. In vitro evolution of proteins. Journal of Bioscience and Bioengineering **6**: 449-456.

McCullum EO, Williams BA, Zhang J, Chaput JC. 2010. Random mutagenesis by error-prone PCR. Methods in Molecular Biology **2010**:103-109

Menezes ME, Bhatia S, Bhoopathi P, Das SK, Emdad L, Dasgupta S, Dent P, Wang XY, Sarkar D, Fisher PB. 2014. MDA-7/IL-24: multifunctional cancer killing cytokine. Advances in Experimental Medicine and Biology **2014**:127-153.

Menezes ME, Bhoopathi P, Pradhan AK, Emdad L, Das SK, Guo C, Wang XY, Sarkar D, Fisher PB. 2018. Role of MDA-7/IL-24 a Multifunction Protein in Human Diseases. Advanced Cancer Research **138**:143-182.

Miles JA, Hobor F, Trinh CH, Taylor J, Tiede C, Rowell PR, Jackson BR, Nadat FA, Ramsahye P, Kyle HF, Wicky BIM, Clarke J, Tomlinson DC, Wilson AJ, Edwards TA. 2021. Selective Affimers Recognise the BCL-2 Family Proteins BCL-xL and MCL-1 through Noncanonical Structural Motifs. ChemBioChem **22**:232-240.

Mirlekar B. 2022. Tumor promoting roles of IL-10, TGF-β, IL-4, and IL-35: Its implications in cancer immunotherapy. SAGE open medicine (35096390) DOI:10.1177/20503121211069012.

Newton MS, Cabezas-Perusse Y, Tong CL, Seelig B. 2020. In Vitro Selection of Peptides and Proteins-Advantages of mRNA Display. ACS Synthetic Biology **9**:181-190.

Nossal GJ. 1967. Mechanisms of antibody production. Annual Review of Medicine **18**:81-96.

Obmolova G, Teplyakov A, Malia TJ, Keough E, Luo J, Sweet R, Jacobs SA, Yi F, Hippensteel R, O'Neil KT, Gilliland GL. 2015. Induced conformational change in human IL-4 upon binding of a signal-neutralizing DARPin. Proteins **83**:1191-1197.

Okonechnikov K, Golosova O, Fursov M. 2012. the UGENE team. Unipro UGENE: a unified bioinformatics toolkit . Bioinformatics **28**:1166-1167.

Ouyang W, O'Garra A. 2019. IL-10 Family Cytokines IL-10 and IL-22: from Basic Science to Clinical Translation. Immunity (30995504) DOI: 10.1016/j.immuni.2019.03.020.

Ouyang W, Rutz S, Crellin NK, Valdez PA, Hymowitz SG. 2011. Regulation and functions of the IL-10 family of cytokines in inflammation and disease. Annual Review of Immunology (21166540) DOI: 10.1146/annurev-immunol-031210-101312.

Persaud L, De Jesus D, Brannigan O, Richiez-Paredes M, Huaman J, Alvarado G, Riker L, Mendez G, Dejoie J, Sauane M. Mechanism of Action and Applications of Interleukin 24 in Immunotherapy. International Journal of Molecular Sciences (27271601) DOI: 10.3390/ijms17060869.

PCR, qPCR, & DNA Amplification. 2022. What is the Role of MgCl2 in PCR? Excer. Available from https://www.excedr.com/resources/what-is-the-role-of-mgcl2-in-pcr/ (accessed January 2023).

Pham PN, Huliciak M, Biedermannova L, Cerny J, Charnavets T, Fuertes G, Herynek S, Kolarová L, Kolenko P, Pavlicek J, Zahradnik J, Mikulecky P, Schneider B. 2021. Protein Binder (ProBi) as a New Class of Structurally Robust Non-Antibody Protein Scaffold for Directed Evolution. Viruses **13**:190-210.

Plückthun A. 2012. Ribosome display: a perspective. Methods in molecular biology **805**:3-28.

Propper DJ, Balkwill FR. (2022). Harnessing cytokines and chemokines for cancer therapy. Nature reviews clinical oncology **19**: 237–253.

Rallis KS, Corrigan AE, Dadah H, George AM, Keshwara SM, Sideris M, Szabados B. 2021. Cytokine-based Cancer Immunotherapy: Challenges and Opportunities for IL-10. Anticancer Research **1**:3247-3252

Ramage R, Green J, Muir TW, Ogunjobi OM, Love S, Shaw K. 1994. Synthetic, structural and biological studies of the ubiquitin system: the total chemical synthesis of ubiquitin. Biochemical Journal **299**:151-8.

Ramamurthy V, Krystek SR Jr, Bush A, Wei A, Emanuel SL, Das Gupta R, Janjua A, Cheng L, Murdock M, Abramczyk B, Cohen D, Lin Z, Morin P, Davis JH, Dabritz M, McLaughlin DC, Russo KA, Chao G, Wright MC, Jenny VA, Engle LJ, Furfine E, Sheriff S. 2012. Structures of adnectin/protein complexes reveal an expanded binding footprint. Structure **20**:259-269.

Ramani T, Auletta CS, Weinstock D, Mounho-Zamora B, Ryan PC, Salcedo TW, Bannish G. 2015. Cytokines: The Good, the Bad, and the Deadly. International Journal of Toxicology **34**:355-365.

Rauth S, Hinz D, Börger M, Uhrig M, Mayhaus M, Riemenschneider M, Skerra A. 2016. High-affinity Anticalins with aggregation-blocking activity directed against the Alzheimer β-amyloid peptide. Biochemical Journal **473**:1563-1578.

Reckel S, Gehin C, Tardivon D, Georgeon S, Kükenshöner T, Löhr F, Koide A, Buchner L, Panjkovich A, Reynaud A, Pinho S, Gerig B, Svergun D, Pojer F, Güntert P, Dötsch V, Koide S, Gavin AC, Hantschel O. 2017. Structural and functional dissection of the DH and PH domains of oncogenic Bcr-Abl tyrosine kinase. Nature **8**: 2101-2115.

Ren C, Wen X, Mencius J. 2019. Selection and screening strategies in directed evolution to improve protein stability. Bioresources and Bioprocessing **6**:53-67.

Rndsystem. 2023. IL-10: Recombinant human IL-10 protein. Rndsystem. Available from https://www.rndsystems.com/products/recombinant-human-il-10-protein_217-il (accessed January 2023).

Direct evolution. 2019. Protein Expression: Methods for tirected evolution of proteins. Sigma-Aldrich. Available from https://www.sigmaaldrich.com/NO/en/technical-documents/technical-article/protein-biology/protein-expression/directed-evolution (accessed November 2022).

Rocha-Junior LF, Branco Pinto Duarte AL, de Melo Rêgo MJB, de Almeida AR, de Melo Vilar K, de Lima HD, Tavares Dantas A, de Ataíde Mariz H, da Rocha Pitta I, da Rocha Pitta MG. 2020. Sensitivity and specificity of Interleukin 29 in patients with rheumatoid arthritis and other rheumatic diseases. Immunology Letters **220**:38-43.

Rogozin IB, Pavlov YI. 2003. Theoretical analysis of mutation hotspots and their DNA sequence context specificity. Mutation Research **544**:65-85.

Ruff AJ, Kardashliev T, Dennig A, Schwaneberg U. 2014. The Sequence Saturation Mutagenesis (SeSaM) method. Methods in Molecular Biology **1179**:45-68.

Sabin C, Plevka P. 2016. The use of noncrystallographic symmetry averaging to solve structures from data affected by perfect hemihedral twinning. Acta Crystallographica Section **72**:188-97.

Seeger MA, Zbinden R, Flütsch A, Gutte PG, Engeler S, Roschitzki-Voser H, Grütter MG. 2013. Design, construction, and characterization of a second-generation DARP in library with reduced hydrophobicity. Protein Science **22**:1239-1257.

Sheehan J, Marasco WA. 2015. Phage and Yeast Display. Microbiology Spectrum (26104550) DOI: 10.1128/microbiolspec.AID-0028-2014.

Schiefner A, Gebauer M, Richter A, Skerra A. 2018. Anticalins Reveal High Plasticity in the Mode of Complex Formation with a Common Tumor Antigen **26**:649-656.

Simeon R, Chen Z. 2018. In vitro-engineered non-antibody protein therapeutics. Protein Cell **9**:3-14.

Smith MR, Khera E, Wen F. 2015. Engineering Novel and Improved Biocatalysts by Cell Surface Display. Industrial & engineering chemistry research **54**:4021-4032.

Smith GP, Petrenko VA. 1997. Phage display. Chemical Reviews **97**:391-410.

Sorensen J, Sandberg D, Sandstrom M, Wennborg A, Feldwisch J, Tolmachev V, Astrom G, Lubberink M, Garske-Roman U, Carlsson J, Lindman H. 2014. First-in-human molecular imaging of HER2 expression in breast cancer metastases using the 111In-ABY-025 affibody molecule. The Journal of Nuclear Medicine **55**:730-735.

Stern LA, Lown PS, Hackel BJ. 2020. Ligand Engineering via Yeast Surface Display and Adherent Cell Panning. Methods in molecular biology **2070**:303-320.

Striz I, Holan V. 2015. Cytokiny v klinicke medicine. Maxdorf, Praha.

Skrlec K, Strukelj B, Berlec A. 2015. Non-immunoglobulin scaffolds: a focus on their targets. Trends in Biotechnology **33**:408-418.

Tabata T, Sugiyama N, Otsuki Y, Kondo Y. 2020. Interleukin-24 is a novel diagnostic biomarker for the severity of acute kidney injury. Medical Molecular Morphology **53**:115-123.

Tanaka T, Kondo A. 2015. Cell-surface display of enzymes by the yeast Saccharomyces cerevisiae for synthetic biology. FEMS Yeast Research **15**:1-9.

Teplyakov A, Malia TJ, Obmolova G, Jacobs SA, O'Neil KT, Gilliland GL. 2017. Conformational flexibility of an anti-IL-13 DARPin. Protein Engineering Design & Selection **30**:31-37.

Vaillant AA, Qurie A. 2022. Interleukin. StatPearls (29763015), DOI: NBK441915.

Vazquez-Lombardi R, Phan TG, Zimmermann C, Lowe D, Jermutus L, Christ D. 2015. Challenges and opportunities for non-antibody scaffold drugs. Drug Discovery Today **20**:1271-1283.

Verma R, Balakrishnan L, Sharma K, Khan AA, Advani J, Gowda H, Tripathy SP, Suar M, Pandey A, Gandotra S, Prasad TS, Shankar S. 2016. A network map of Interleukin-10 signaling pathway. The Journal of Cell Communication and Signaling **10**:61-7.

Wang H, Liu R. 2011. Advantages of mRNA display selections over other selection techniques for investigation of protein-protein interactions. Expert Rev Proteomics **8**:335-346.

Wang H, Vilela M, Winkler A, Tarnawski M, Schlichting I, Yumerefendi H, Kuhlman B, Liu R, Danuser G, Hahn KM. 2016. LOVTRAP: an optogenetic system for photoinduced protein dissociation. Nature Methods **13**:755-758.

Wang YC, Peterson SE, Loring JF. 2013. Protein post-translational modifications and regulation of pluripotency in human stem cells. Cell Research (24217768) DOI: 10.1038/cr.2013.151.

Wilson DS, Keefe AD. 2001. Random mutagenesis by PCR. Current Protocols in Molecular Biology (18265275) DOI: 10.1002/0471142727.mb0803s51.

Wong TS, Tee KL, Hauer B, Schwaneberg U. 2004. Sequence saturation mutagenesis (SeSaM): a novel method for directed evolution. Nucleic Acids Research (e26) DOI: 10.1093/nar/gnh028.

Wong TS, Zhurina D, Schwaneberg U. 2006. The diverzity challenge in directed protein evolution. Combinatorial Chemistry & High Throughput Screening **9**:271-288.

Worrall AF. 1994. Site-directed mutagenesis by the cassette method. Methods in Molecular Biology **30**:199-210.

Yang L, Arora K, Beard WA, Wilson SH, Schlick T. 2004. Critical role of magnesium ions in DNA polymerase beta's closing and active site assembly. Journal of the American Chemical Society **126**:8441-8453.

Yang Y, Chen J, Yi C, Yang F, Tang M, Li Z, Bai X. 2022. Assessment of serum interleukin-28 as a biomarker to predict mortality in traumatic patients with sepsis. Cytokine (35816926) DOI: 10.1016/j.cyto.2022.155959.

Yao Z, Jeon HS, Yoo JY, Kang YJ, Kim MJ, Kim TJ, Kim JH. 2022. DNA Shuffling of aprE Genes to Increase Fibrinolytic Activity and Thermostability. Journal of Microbiology and Biotechnology **32**:800-807.

World Health Organization. 2022. Fact sheets: Cancer. Available from https://www.who.int/news-room/fact-sheets/detail/cancer (accessed March 2022).

World Health Organization. 2020. Health topics: Cardiovascular diseases. Available from https://www.who.int/health-topics/cardiovascular-diseases#tab=tab_1 (accessed March 2022).

Zahnd C, Amstutz P, Pluckthun A. 2007. Ribosome display: selecting and evolving proteins in vitro that specifically bind to a target. Nature Methods **4**:269-79.

Zhao H. 2004. Staggered extension process in vitro DNA recombination. Methods in Enzymology **388**:42-49.

Zahradnik J, Dey D, Marciano S, Kolarova L, Charendoff CI, Subtil A, Schreiber G. 2021. A Protein-Engineered, Enhanced Yeast Display Platform for Rapid Evolution of Challenging Targets. ACS Synthetic Biology **10**:3445-3460.

Zheng D, Aramini JM, Montelione GT. 2004. Validation of helical tilt angles in the solution NMR structure of the Z domain of Staphylococcal protein A by combined analysis of residual dipolar coupling and NOE data. Protein Science **13**:549-554.

9 Appendix

9.1 Appendix I
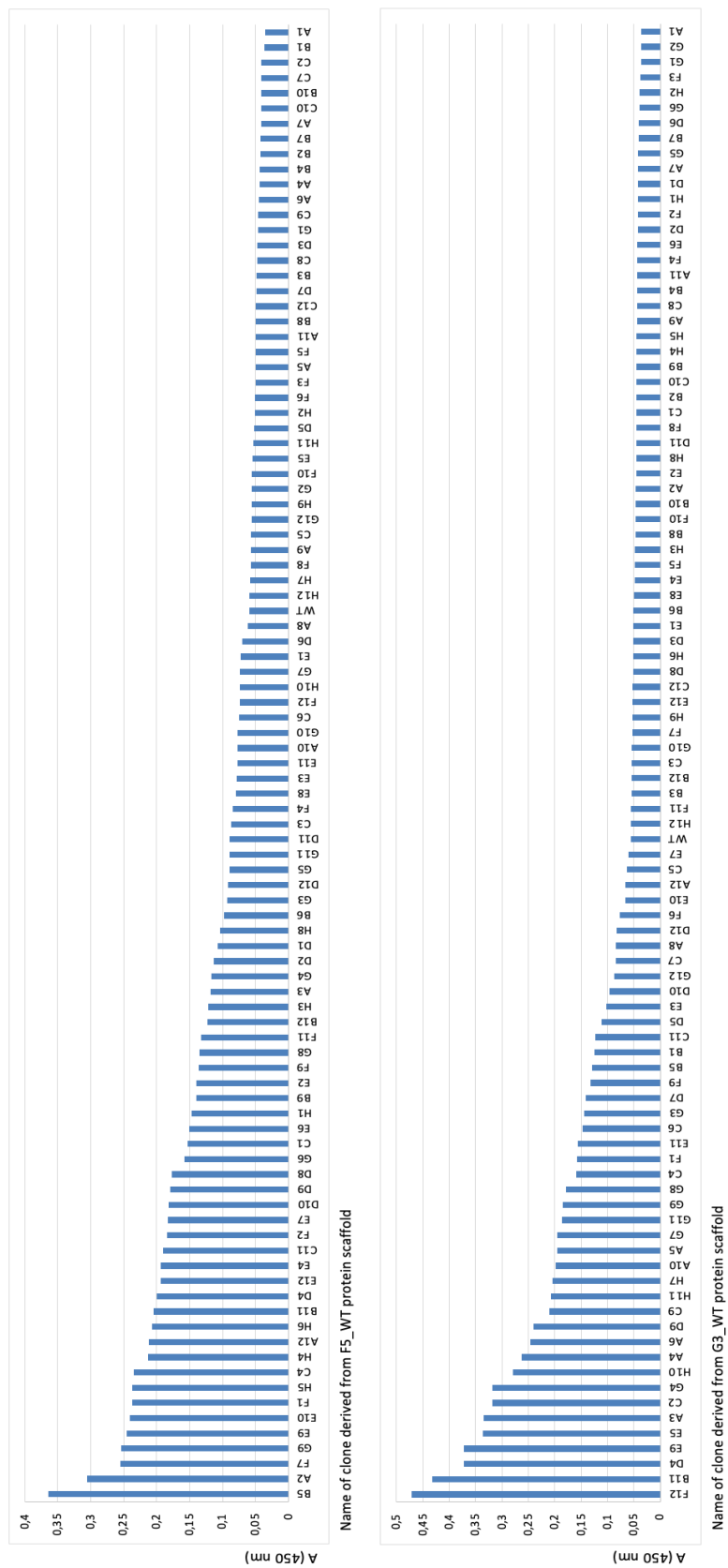
Figure A1: Absorbance values of clones derived from F5_WT and G3_WT by error-prone PCR, ribosome display and ELISA screenig selection methods.

9.2   Appendix II

Figure A2: Sequence alignment of variants derived from F5_WT and G3_WT via error-prone PCR diversification (mutated amino acids are highlighted in light blue color).

Figure A3: Sequence alignment of variants derived from F5_WT and G3_WT via error-prone PCR diversification, Ribosome display and ELISA screening selection methods selection (mutated amino acids are highlighted in light blue color).

9.3 Appendix III

Table A1: Concentrations of isolated plasmid DNA with DNA construct pMTH-NiP-IL10-Chris ($A_{260/230}$ ratio is used for measurement purity of DNA, Andix$_{pe}$ratio for secondary measurement of nucleic acid purity).

c [ng/µl]	A $_{260/230}$	A $_{260/280}$
6633.6	2.3	1.8

Table A2: Concentrations of isolated plasmid DNA with DNA constructs PETsm and PRDVsm ($A_{260/230}$ ratio is used for measurement purity of DNA, $A_{260/280}$ ratio for secondary measurement of nucleic acid purity).

Name of plasmid	c[ng/µl]	A $_{260/230}$	A $_{260/280}$
PETsm	265.2	2.2	1.8
PRDVsm	320.4	2.2	1.8

Table A3: Concentrations of amplificated clones F5_WT and G3_WT

Name of DNA fragment	c[ng/µl]
F5_WT	30.2
G3_WT	13.4

Table A4: Concentrations of plasmid DNA with tranformed constructs pRDVsm_F5_EP/G3_EP ($A_{260/230}$ ratio is used for measurement purity of DNA, $A_{260/280}$ ratio for secondary measurement of nucleic acid purity).

Name of plasmid	c[ng/µl]	A $_{260/230}$	A $_{260/280}$	Name of plasmid	c[ng/µl]	A $_{260/230}$	A $_{260/280}$
A/1	61.2	2.2	1.8	D/1	81.0	1.9	1.8
A/2	69.6	2.1	1.7	D/2	58.8	1.7	1.7
A/3	84.1	1.7	1.6	D/3	64.1	2.0	1.8
A/4	71.4	1.7	1.7	D/4	58.0	2.1	1.8
A/5	62.2	2.0	1.7	D/5	126.8	2.0	1.8
B/1	70.0	2.1	1.8	E/1	61.3	2.0	1.8
B/2	65.0	2.1	1.8	E/2	66.0	2.2	1.8
B/3	72.8	2.1	1.8	E/3	124.4	2.0	1.8
B/4	64.5	1.9	1.7	E/4	145.1	2.1	1.8
B/5	58.5	2.2	1.7	E/5	53.5	2.1	1.8
C/1	63.3	2.0	1.7	F/1	64.0	2.1	1.8
C/2	65.0	1.9	1.8	F/2	49.8	2.3	1.8
C/3	66.1	1.6	1.8	F/3	62.0	2.1	1.8
C/4	66.0	1.6	1.7	F/4	54.7	2.3	1.8
C/5	63.2	1.7	1.7	F/5	46.4	2.0	1.8

Table A5: Concentrations of isolated DNA products RD_F5$_{EP}$ and RD_G3$_{EP}$ (A$_{260/230}$ ratio is used for measurement purity of DNA, A$_{260/280}$ ratio for secondary measurement of nucleic acid purity).

Name of DNAfragment	c [ng/µl]	A $_{260/230}$	A $_{260/280}$
RD_F5$_{EP}$	75.7	1.4	1.8
RD_G3$_{EP}$	79.3	1.6	1.7

Table A6: Concentrations of the best scaffold candidates selected by ELISA screening

Name of plasmid	c [ng/µl]	A $_{260/230}$	A $_{260/280}$	Name of plasmid	c [ng/µl]	A $_{260/230}$	A $_{260/280}$
F5_A2	117.4	2.1	1.8	G3_A3	56.8	2.0	1.8
F5_A12	115.0	2.3	1.8	G3_A4	66.0	2.3	1.8
F5_B5	122.6	2.3	1.8	G3_A6	63.4	2.3	1.8
F5_B11	128.5	2.2	1.8	G3_B11	83.2	2.3	1.8
F5_C4	118.7	2.3	1.8	G3_C2	76.8	2.0	1.8
F5_E9	115.7	2.3	1.8	G3_D4	83.5	2.0	1.8
F5_F1	108.0	2.3	1.8	G3_D9	58.0	2.2	1.7
F5_F7	99.3	2.2	1.8	G3_E5	86.4	2.3	1.8
F5_G9	78.1	2.3	1.8	G3_F12	88.9	2.3	1.8
F5_H4	106.6	2.3	1.8	G3_E9	63.2	2.2	1.8
F5_H5	103.1	2.3	1.8	G3_G4	73.7	2.1	1.8
F5_H6	91.5	2.2	1.8	G3_H10	58.7	2.3	1.8

9.4 Appendix IV

Preparation of amino acid sequences for alignment

```python
# Required libraries imported
from Bio import SeqIO
from Bio.Seq import Seq
from Bio.Seq import translate
from Bio.SeqRecord import SeqRecord
import os

# Read F5 wildtype amino acid sequence from .txt file
with open("F5/F5_wildtype.txt", "r") as file_f5_wt:
    F5_wildtype_str = file_f5_wt.readlines()[0]

# Prepare sequences for aligning
F5_list_to_align = []
# The wildtype is first member of the list
F5_list_to_align.append(SeqRecord(Seq(F5_wildtype_str), id="F5_wt"))
# read F5 clone files containing sequences of nucleotides
for file in os.listdir("F5"):
    if file.endswith(".ab1"):
        handle = open("F5/" + file, "rb")
        for record in SeqIO.parse(handle, "abi"):
            # Translate the nucleotide sequence to amino acid sequence
            sequence = translate(record._seq)
        seq_name = file[:6]
        # Append to the list of amino acid sequences
        F5_list_to_align.append(SeqRecord(sequence, id=seq_name))

# List of amino acid sequences saved to .fasta file in FASTA format.
SeqIO.write(F5_list_to_align, "F5_sequences_for_alignment.fasta", "fasta")


# read G3 wildtype amino acid sequence from .txt file
with open("G3/G3_wildtype.txt", "r") as file_G3_wt:
    G3_wildtype_str = file_G3_wt.readlines()[0]

# Prepare sequences for aligning
G3_list_to_align = []
# The wildtype is first member of the list again
G3_list_to_align.append(SeqRecord(Seq(G3_wildtype_str), id="G3_wt"))
# read G3 clone files containing sequences of nucleotides
for file in os.listdir("G3"):
    if file.endswith(".ab1"):
        handle = open("G3/" + file, "rb")
        for record in SeqIO.parse(handle, "abi"):
            # Translate the nucleotide sequence to amino acid sequence
            sequence = translate(record._seq)
        seq_name = file[:6]
        # Append to the list of amino acid sequences
        G3_list_to_align.append(SeqRecord(sequence, id=seq_name))

# List of sequences saved to .fasta file in FASTA format.
SeqIO.write(G3_list_to_align, "G3_sequences_for_alignment.fasta", "fasta")
```

9.5 Appendix V

Calculation of properties of aligned proteins

```python
# Required libraries imported
from Bio import SeqIO
from Bio.Seq import Seq
from Bio.Seq import translate
from Bio.SeqRecord import SeqRecord
from Bio.SeqUtils.ProtParam import ProteinAnalysis
import numpy as np
import pandas as pd
import openpyxl
import os

# F5 clones
f5_dict = {}
# After alignation, for wildtype and each clone varius properties are calculated
for record in SeqIO.parse("F5_aligned_sequences.fasta", "fasta"):
    protein_dict = {}
    # Read the protein
    protein = ProteinAnalysis(str(record.seq._data)[2:-1])
    # Calculate the properties
    protein_dict["GRAVY"] = protein.gravy()
    # Insert the information into dictionary of proteins
    f5_dict[record.id] = protein_dict

# G3 clones
g3_dict = {}
# After alignation, for wildtype and each clone varius properties are calculated
for record in SeqIO.parse("F5_aligned_sequences.fasta", "fasta"):
    protein_dict = {}
    # Read the protein
    protein = ProteinAnalysis(str(record.seq._data)[2:-1])
    # Calculate the properties
    protein_dict["GRAVY"] = protein.gravy()
    # Insert the information into dictionary of proteins
    g3_dict[record.id] = protein_dict


# The dictionaries can be transformed to DataFrames
f5_df = pd.DataFrame.from_dict(f5_dict, orient="index")
g3_df = pd.DataFrame.from_dict(g3_dict, orient="index")

# For each parameter, we can calculate mean value of clones and compare them to values of
wildtype.
for param in f5_df.columns:
    if param == "charge_at_pH":
        continue
    f5_wt = f5_df[param].values[0]
    f5_rest = f5_df[param].values[1:8]
    # Mean
    f5_rest_mean = f5_rest.mean()
    # Standard deviation
    f5_rest_std = f5_rest.std()
    # 95% Condifence interval width (for two-sided test)
    f5_interval_width = 2.447 * f5_rest_std / np.sqrt(6)
    f5_interval = (f5_rest_mean - f5_interval_width, f5_rest_mean + f5_interval_width)
    f5_in_interval = f5_wt > f5_interval[0] and f5_wt < f5_interval[1]

    f5_df.loc["mean", param] = f5_rest_mean
    f5_df.loc["int_min", param] = f5_interval[0]
    f5_df.loc["int_max", param] = f5_interval[1]
    # If wildtype value is outside of the confidence interval,
    # we can reject hypothesis that mean value of clones is equal to value of wildtype.
    f5_df.loc["sig_diff", param] = not f5_in_interval

    # Previous procedure repeated for G3 wildtype and corresponding clones.
    g3_wt = g3_df[param].values[0]
    g3_rest = g3_df[param].values[1:7]
    g3_rest_mean = g3_rest.mean()
    g3_rest_std = g3_rest.std()
    g3_interval_width = 2.365 * g3_rest_std / np.sqrt(7)
    g3_interval = (g3_rest_mean - g3_interval_width, g3_rest_mean + g3_interval_width)
    g3_in_interval = g3_wt > g3_interval[0] and g3_wt < g3_interval[1]
```

```python
        g3_df.loc["mean", param] = g3_rest_mean
        g3_df.loc["int_min", param] = g3_interval[0]
        g3_df.loc["int_max", param] = g3_interval[1]
        g3_df.loc["sig_diff", param] = not g3_in_interval

# Export results to .xslx file.
with pd.ExcelWriter("f5_g3_params.xlsx") as writer:
    f5_df.to_excel(writer, sheet_name="F5")
    g3_df.to_excel(writer, sheet_name="G3")
```